Joakim Hegg Johansen

Non-linear control and digital twin modeling of the REMUS 100 AUV.

Sliding mode control in 6 DOF and digital twin exploration.

Master's thesis in Marine Cybernetics

Supervisor: Dong Trong Nguyen

June 2020

Master's thesis

NTNU
Norwegian University of Science and Technology
Faculty of Engineering
Department of Marine Technology

NTNU
Norwegian University of
Science and Technology

Abstract

Operating autonomous underwater vehicles (AUV) in harsh, remote environments involves the risk of collisions and loss of assets. Highly coupled and non-linear dynamics combined with under-actuation and uncertainties in hydrodynamics makes the control of AUVs challenging. Therefore, comprehensive testing of the control system is crucial and necessary before deploying it to the physical AUV.

To deal with these demanding operating conditions, various control schemes have been developed for underwater vehicles. This thesis presents a robust, non-linear control algorithm in 6 degrees of freedom (DOF) for the REMUS 100 AUV using the sliding mode (SMC) methodology. Such an algorithm would make the REMUS 100 capable of executing complex missions while being affected by environmental disturbances and model uncertainties. A Simulink simulator is used to design the control law and test its performance. Further, a comparison between the SMC and the existing controller of the REMUS 100 is presented.

A digital twin (DT) is a digital replica of a physical asset and a bridging between the physical and virtual world. In the development phase of a control system, a DT would provide testing and optimization without the risk of damaging the real asset, thus reducing the cost. Using the Core Simulation Environment (CSE) demo application a numerical DT of the REMUS 100 is created to further test the SMC and explore the benefits of DTs.

Results from the simulation suggest that the SMC is a suitable control scheme for underwater vehicles such as the REMUS 100, but that further tests are needed before deploying the algorithm to the physical asset. Moreover, the possibilities DTs present are many and will only increase with time.

Sammendrag

Bruken av autonome undervannsfarkoster (AUV) i krevende, avsidesliggende miljøer involverer risikoen for kollisjoner og tap av fartøy. Koblet og ulineær dynamikk kombinert med underaktuering og usikker hydrodynamikk gjør kontroll av AUVer utfordrende. Grundig testing av kontrollsystemet er derfor viktig og nødvendig før det distribueres til den fysiske AUVen.

Mange kontroll algoritmer har blitt utviklet for å håndtere de krevende driftsforholdene undervannsfartøy operer i. Denne oppgaven presenterer en robust, ulineær kontroll algoritme i 6 frihetsgrader for REMUS 100 AUVen ved å bruke sliding mode (SMC) metoden. En slik algoritme vil gjøre REMUS 100 i stand til å utføre komplekse oppdrag mens den er påvirket av forstyrrelser og usikkerhet i modellen. En Simulink simulator er brukt for å designe kontroll loven og teste prestasjonen. Videre er en sammenligning mellom SMC og den nåværende kontrolleren som brukes av REMUS 100 presentert.

En digital tvilling (DT) er en digital kopi av en fysisk gjenstand og en kopling mellom den fysiske og virtuelle verden. I utviklingsprosessen for et kontrollsystem kan en DT brukes til å teste og optimalisere systemet uten å risikere å skade fartøyet, noe som vil redusere kostnadene. Ved å bruke en demo av Core Simulation Environment (CSE) vil en numerisk DT av REMUS 100 lages for å ytterlige teste SMC algoritmen og utforske fordelene ved DTer.

Resultatene fra simuleringen tilsier at SMC er en passende algoritme for undervannsfarkoster som REMUS 100, men at ytterlige tester må gjennomføres før algoritmen brukes på det fysiske fartøyet. Videre er mulighetene DTer presenterer mange og vil bare øke med tiden.

Acknowledgements

I want to thank my supervisor, Dong Trong Nguyen, for devoting time and resources to help me as much as possible during my work with this thesis.

Further, I want to thank Kristoffer Eide, Ramos de Carvalho, and Cesar Augusto from DNV-GL for giving me the necessary introduction to CSE. Lastly, I would also like to thank Petter Norgren and the rest of the AUR Lab at NTNU for inviting me to participate in a field trip involving the REMUS 100.

Abbreviations

ASB	=	The Adaptive Control Law of Slotine and Benedetto
ASE	=	Analytical and Semi-Empirical
ASMC	=	Adaptive Sliding Mode Control
AUV	=	Autonomous Underwater Vehicle
AUR	=	Applied Underwater Robotics
CB	=	Center of Buoyancy
CFD	=	Computational Fluid Dynamics
CG	=	Center of Gravity
CO	=	Center of Orientation
CSE	=	Core Simulation Environment
DCAL	=	The Adaptive Control Law of Sadegh and Horowitz
DOF	=	Degree of Freedom
DT	=	Digital Twin
EAVE	=	Experimental Autonomous Vehicle
E.O.M	=	Equations of Motion
FMI	=	Functional Mock-up Interface
FMU	=	Functional Mock-up Unit
GUI	=	Graphical User Interface
LQR	=	Linear Quadratic Regulator
LQG	=	Linear Quadratic Gaussian
NED	=	North East Down
OSP	=	Open Simulation Platform
PID	=	Proportional, Integral, Derivative
REMUS	=	Remote Environmental Monitoring UnitS
ROV	=	Remotely Operated Vehicle
SMC	=	Sliding Mode Control
SNUUV	=	Seoul National University Underwater Vehicle
SPURV	=	Special Purpose Underwater Research Vehicle
UARS	=	Unmanned Arctic Research Submersible
UAV	=	Unmanned Aerial Vehicles

Table of Contents

List of Figures

List of Tables

Chapter 1

Introduction

In this chapter, the background and motivation for this thesis are presented. Further, the objective and scope, as well as the contribution and outline of the thesis are given.

1.1 Background

An AUV is an unmanned underwater vehicle capable of self-propulsion. It is driven through the water using a propulsion system and uses fins and rudders to move in 6 DOF [1]. The use of AUVs in subsea operations could be an answer to the exploration and exploitation of challenging areas, such as deeps seas and harsh Arctic environments. Replacing humans in such environments will improve safety and increase performance by reducing human errors.
A digital twin (DT) is a virtual model of a process, product, or service. This pairing of the virtual and physical worlds could, through analysis of data and monitoring of systems, make it possible to detect problems before they even occur, minimize downtime, develop opportunities and plan for the future using simulations [2].

1.1.1 Motivation

Given their autonomous nature, AUVs are dependent on robust and reliable control algorithms to achieve optimal performance. The design of such systems is challenging and a large number of control laws exist. Without proper testing, the consequences of a faulty control system can be fatal and expensive. Using a DT of an AUV in the design process of the control algorithm it would be possible to test the algorithm before deploying it to the physical asset. This would enable optimization of the control algorithm, thus drastically reduce the cost and chance of error. During the operation phase, a DT would also help optimize the operation process and monitor the asset to diagnose possible errors before they occur.
The REMUS (Remote Environmental Monitoring UnitS) 100 is an AUV used by the AUR (Applied Underwater Robotics) Lab at NTNU to map the seabed in the Trondheim Fjord.

Through conversations with Petter Norgren, a Postdoc for AUR Lab, it became clear that unwanted roll-angle was an occurring problem for the REMUS 100. The creation of a DT of the REMUS 100 could help optimize the current operation through a better, more suitable, and robust control algorithm.

1.1.2 REMUS 100

The REMUS 100 was designed by the Woods Hole Oceanographic Institution and manufactured by the spinoff company Hydroid Inc, a wholly-owned subsidiary of Kongsberg Maritime.
The capabilities of the REMUS 100 make it suitable for marine research, defense, hydrographic, and offshore/energy markets. Its main applications include scientific mapping, under ice exploration, mine counter exploration and pipeline survey [3].

Figure 1.1: The REMUS 100 AUV

Propulsion is done by a single propeller and steering is controlled by two stern planes (horizontal fins) and two rudder planes (vertical fins), controlling pitch and heading, respectively.

1.2 Objective and Scope

1.2.1 Objective

The first objective of this thesis is to design a robust, non-linear control algorithm for the REMUS 100 in 6 DOF capable of dealing with model uncertainties and environmental disturbances. Numerous control algorithms exist, thus a thorough literature review exploring the pros and cons, as well as experiments involving different control methodologies on underwater vehicles, is necessary. A Simulink simulator will be used to test the designed control law. The controller will also be compared to the current REMUS 100 control algorithm by comparing results collected from an executed field trip with simulation results.

The second objective is to create a DT of the REMUS 100 using CSE. The goal is to create a simulation environment for the REMUS 100 where it's easy to analyze and optimize the control system, as well as other parts of the system. The general benefits and downsides of DTs will also be explored and discussed. Additionally, relevant literature regarding the mathematical modeling of AUVs and the use of DTs in subsea operations will be reviewed.

1.2.2 Scope

Scope of work:

1. Perform a background and literature review to provide information and relevant references on:
    - DTs in subsea operations
    - AUVs in subsea operations
    - Mathematical modeling of AUVs
    - Control of AUVs
2. Propose mathematical modeling of the REMUS 100.
3. Design a robust, non-linear control algorithm for the REMUS 100 in 6DOF and implement it in a Simulink simulator of the AUV.
4. Test the designed controller's ability to follow a predetermined trajectory while being exposed to currents.
5. Discuss the designed control law and compare it to the control law currently being used by the REMUS 100.
6. Create a DT of REMUS 100 using CSE.
7. Run simulations using the DT and discuss the benefits/drawbacks compared to regular Simulink simulations.
8. Conclude and propose ideas for further work.

1.3 Contribution

Even though the field of AUV control is well documented, most of the papers propose decoupling of the dynamics into subsystems for speed/heading/depth or in the longitudinal/lateral plane. Few efforts have been made to achieve control of the non-linear dynamics in 6 DOF. One contribution of this thesis is a robust sliding mode controller (SMC) capable of dealing with the highly coupled and non-linear dynamics of the REMUS 100 in 6 DOFs. The designed controller could serve as a good alternative to the control law used by the REMUS 100 today.
Other contributions are the creation of a numerical DT of the REMUS 100, as well as an exploration of the benefits a DT can provide. Moreover, the created DT can be used by others working with the REMUS 100 for further research and exploration of the topic. A thorough litterateur review is also presented.

1.4 Outline of the thesis

Chapter 2 summarizes a comprehensive literature review and discuss the findings. The use of DT in subsea operations is first examined, followed by a summary of the history of AUVs. Then a more thorough review is done on the mathematical modeling and control of AUVs.

Chapter 3 presents the general mathematical model for AUVs and the SMC method. This is followed by the implementation of these theories, as well as a simple guidance system, for the REMUS 100 Simulink simulator. Lastly, the method for creating the DT is given.

Chapter 4 discusses the designed controller and compares it to the current REMUS 100 control algorithm. Simulations using the DT are also presented and discussed.

Chapter 5 concludes the thesis and suggests ideas for further work.

Appendix A presents the numerical coefficients for the REMUS 100 used in the Simulink simulator.

Appendix B outline Barbalat's lemma.

Appendix C describes the attached zip-file containing files used to run the Simulink simulation, as wells as building the DT.

Chapter 2

Literature Review

In this chapter, a search and evaluation of the available literature on the relevant subjects are given. The objectives are to present the literature in an organized way, identify gaps in current knowledge, and critically analyze the information gathered to better execute this project. The reviewed topic areas are:

- Digital Twins in subsea operations, 2.1
- AUVs in subsea operations, 2.2.1
- Mathematical modeling of AUVs, 2.2.2
- Control of AUVs, 2.2.3

2.1 Digital Twins in subsea operations

A DT is a digital replica of a living or non-living physical entity. By bridging the physical and virtual world, data is transmitted and seamlessly allowing the virtual entity to exist simultaneously with the physical entity [4].
The offshore industry has several technical and commercial challenges including reduction of cost and trying to achieve superior returns of investment. The economic value derived from a DT will be evident from the improved productivity, efficiency, safety, transparency, and confidence to users and clients [5].
Subsea operation's challenges, particularly in deepwater, make DT solutions very convenient. Even the slightest improvement to inspection regimes can deliver significant safety, efficiency, and cost benefits. With an established, robust, and proved DT of the asset in place, the traditional method of inspection can be transformed. Instead of sending an inspector offshore to operate the remotely operated vehicle (ROV) for inspection, the inspector can sit onshore using the DT [6].

DTs are today considered as more than just a collection of digital artifacts, but rather as collections of linked digital artifacts. The integration and linking of the model and the data are key. It is argued that the value of DTs primarily lies in the elimination of information inefficiencies which results in a waste of resources. [7] demonstrated how the integrated model adds value to different stages of the lifecycle, allowing evaluation of performance in the design phase and real-time reflection of the physical asset during its operation.
In [8] a data-driven DT of a ship was built, leveraging on the large amount of information collected from the on-board sensors, and was used to estimate the speed loss due to marine fouling. Results clearly showed the effectiveness of the proposal and its improved speed loss prediction accuracy, which in return reduced the fuel consumption. It's also concluded that the application of DTs also could be exploited for evaluating the effectiveness of different energy-saving solutions, such as the case of new propeller design.

[9] discussed the increased focus on the development and adoption of AUVs, and how the market is seeing significant growth. The article concluded that autonomous technology is bringing undersea operations into the digital fold and that the days of spending multiple years in development and testing is over. In commercial sectors, patching, updates, and feature roll-outs can happen weekly. With AUVs consisting of complex software and data gathering tools, it is expected that the industry starts paying more attention to the possibilities DTs would provide. The biggest issue for AUVs is the transmission of real-time data from the asset to the DT system. Compared to a stationary oil platform an AUV is in constant motion and below the surface, thus making detailed measurement unavailable. The introduction of 5G could turn out to be the catalyst in the pursuit of high fidelity real-time DTs of AUVs and other underwater vehicles. Providing ultra-high-speed, 5G will offer low latency transmissions we don't have today [10].
Digital twin technology is being explored by most companies within the offshore sector today. By the end of 2020 Open Simulation Platform, or OSP for short is scheduled to launch. The project co-founders DNV-GL, Kongsberg Maritime, NTNU, and Sintef Ocean hope for OSP to establish the standards for models and simulations in the maritime industry, enabling both re-use of models and collaborative system simulations to solve challenges in design, building, and operation of today's and tomorrow's ships [11]. The Core Simulation Environment (CSE) is a co-simulation software application built on a combination of technical solutions from the OSP initiators and other established industrial solutions [12]. When finished, CSE will be an open-source application as part of the initiator's efforts for standardization and inseparability between modeling tools and platforms.

2.2 Autonomous Underwater Vehicles

2.2.1 AUVs in subsea operations

According to [13], the origin of the AUVs should be linked to Whitehead's automobile "Fish" Torpedo, which was designed, built, and presented in Austria in 1886. It was named after the Torpedo fish and could achieve a speed of over 3.0 m/s and run for 700m. Not many AUV-like applications were invented until the Applied Physics Laboratory at the

University of Washington in 1957 deployed the "Special Purpose Underwater Research Vehicle", or SPURV for short [14]. The SPURV was used to study diffusion, acoustic transmissions, and submarine wakes.
During the 1970s multiple testbeds were developed. The University of Washington, in addition to the SPURV, launched the Unmanned Arctic Research Submersible (UARS) to gather data from the Arctic regions. The University of New Hampshire's Marine Systems Engineering Laboratory developed the Experimental Autonomous Vehicle (EAVE) vehicle in cooperation with the US Navy's facility in San Diego. At this time, the Institute of Marine Technology Problems at the Russian Academy of Sciences also began their AUV program and designed the first deep-diving AUVs [15].
Further, [15] emphasized the importance of the introduction of small, low power computers with memory. This made it possible to implement complex guidance and control algorithms on autonomous platforms. An effort was put into understanding how to give an AUV a level of intelligence necessary to accomplish assigned tasks, such as mission planning, perception, and situation assessment. In the USA, research programs were initiated providing funding to develop a proof of concept prototypes. The most noticeable published program being the one at Draper Labs which led to two large AUVs to be used as testbeds for several Navy programs.
During the 90s the AUVs grew from proof of concept testbeds into first-generation operational systems able to execute defined tasks. Multiple organizations across the world undertook development efforts focusing on various objectives. In the early 2000s, several commercial applications for AUVs becoming obvious, according to [15]. The AUV technology moved from the academic environment evolving around research, into the commercial mainstream of the offshore industry.
Today the biggest market for AUV systems is the military, mostly being used for mine countermeasures in very shallow water. The technological progress of the last years combined with the introduction of artificial intelligence and machine learning has resulted in an improvement of the endurance, communications, navigation, and imaging of the AUV systems [16]. The downturn in the oil price also meant that operators had to seek more efficient ways to operate and AUV systems were and remain part of the solution. [16] predicts a future of the subsea industry dominated by large AUV systems and AUV swarms.

2.2.2 Mathematical modeling of AUVs

The mathematical modeling of AUVs is the study of hydrostatic and dynamic forces acting on the vehicle body. The hydrostatics describes the equilibrium of the body at rest or while moving with constant velocity and is based on Archimedes' principle. When the body has an accelerated motion, we talk about the dynamics. Dynamic models of the AUV are the basis for the controller design of the vehicle and is therefore very important to ensure good control performance. In [17] the vehicle dynamics were divided into two parts: kinematics, treating only geometrical aspects of motion, and kinetics, which is the analysis of the forces causing the motion.
In [18] the ROV kinematics were described using two orthogonal coordinate systems, one global, fixed to the ocean surface (mother ship), and one local, which is fixed on the vehicle body. Today, the most used kinematic notation is the one presented by Fossen in [17], where three earth-centered reference frames and three body-fixed reference frames

are presented. In the same book, the AUV kinetics were also thoroughly discussed. The AUV equations of motion were derived through a comprehensive study of the rigid body motions, hydrodynamics, and hydrostatics.

[18] also described underwater vehicle kinetics and put an emphasis on the importance of added mass and introduced functional terms which are essential in describing the equations of motion of an AUV.

The mathematical modeling of an AUV is a set of six nonlinear, time-varying differential equations with many poorly known parameters. The hydrodynamic parameters, and in particular the viscous damping due to drag forces, are difficult terms to model. This has resulted in most models using rough approximations [17]. The hydrodynamic parameters may be identified through expensive hydrodynamic testing on the vehicle. Since the unsteady fluid motion effects are not taken into consideration, it is difficult to derive the complete dynamic model, even when performing physical tests. An example of a hydrodynamic test can be seen in [19] where the testing of the Marine Utility Vehicle System (MARIUS) AUV is presented.

[20] described the development and verification of a 6 DOF, non-linear simulation model for the REMUS 100 AUV. The external forces and moments resulting from hydrostatics, hydrodynamic lift, and drag, added mass, and the control inputs of the vehicle fins and propeller are all defined in terms of vehicle coefficients. The derivation of these is achieved through numeric integration of the equations of motion (E.O.M) followed by an adjustment based on comparisons of experimental data.

Another approach used is predictive models. Considering the unavailability of the vehicle during the design stage and the cost of physical testing, this approach is very attractive. In [21] analytical and semi-empirical (ASE) and computational fluid dynamics (CFD) was used to predict the hydrodynamic derivatives of the MAYA AUV. Using experimental data to compare the numerical results, [22] also showed that the use of CFD is an accurate approach for calculating the hydrodynamic coefficients.

[23] derived a component-based model for the dynamics in a way that only requires the specification of the vehicle geometry and the lift and drag characteristics of its constituent elements. Since the use of hydrodynamic derivatives is avoided by calculating the hydrodynamic coefficients using well-know empirical relations, it's described as a simplified model. Despite being simplified the approach proposed in [23] retains the nonlinear coupled behavior of the vehicle and yield a good result when compared to experimental data. In [24] Prestero derived the vehicle dynamics of the REMUS 100 AUV by combining theory and empirical data. Just like in [23], the hydrodynamic lift and drag and added mass were defined in terms of hydrodynamic coefficients. The difference between the two experiments is Prestero's model of forces and moments acting on the vehicle is more complex, thus making his model more accurate.

The Kalman filter also shows great promise in determining the hydrodynamic derivatives of AUVs. [25] discussed in practical terms the convergence criteria of the Kalman filter, and validated the mathematical model to calculate the hydrodynamic derivatives. In [26] the hydrodynamic coefficient of the Seoul National University Underwater Vehicle (SNUUV) AUV was determined by applying the extended Kalman filter and potential theory, while in [27] a method using a discrete Kalman filter with fading memory combined with the maximum likelihood method were presented.

2.2.3 Control of AUVs

The motion control of AUVs is difficult to achieve autonomously due to various reasons. The AUV often being an under-actuated system, non-linear dynamics, uncertainties in hydrodynamics, and presence of disturbances such as currents, underwater structures, and observational noises are some.
Various types of control algorithms exist, all with advantages and disadvantages. As a rule of thumb, we can divide them into two main groups; linear and non-linear. Linear approaches include the PID-controller [28] [29] [30], the linear quadratic regulator (LQR) controller [31] and the linear quadratic Gaussian (LQG) controller [32].
Non-linear solutions include sliding mode control (SMC) [33] [30], back-stepping techniques [34], adaptive control [35] [36] [37], predictive control [38], and fuzzy logic control [39] [40].

A popular approach for linear control is dividing the 6 DOF differential E.O.M into three non-interacting subsystems for speed control, steering control, and depth control. In [41] the speed (u) was controlled using a PI control law, while a PD-controller was used for steering (v, r, ψ) and depth (w, q, θ, z) control. In [42] the same subsystems were used, but the speed, steering, and depth where controlled by a P, PI, and PPI(P outer loop, PI inner loop) - controller, respectively. The same subsystems can be controlled by an LQR controller as well. [38] compares the proposed PID controller with an LQR controller, concluding with the LQR scheme being the superior linear controller of the two. In [31] a reduced-order system with dive plane dynamics has been derived and linearized for implementing an LQR control strategy for depth control, also yielding good results.
Another approach to deal with the higher dimensional nonlinear model is to use two independent reduced models. One to represent motion dynamics in the horizontal plane and the other for the vertical plane. In [38] this is done by neglecting weakly coupled dynamics between the planes and creating two independent constrained optimization problems. This is also the method used in [43] when designing autopilots for unmanned aerial vehicles (UAVs). The disadvantage of this is that you lose the coupling between the states of the two planes, thus limiting the performance of the controller.

The major disadvantage of linear controllers is that they are unable to account for the non-linearities of the system. Since the underwater vehicle dynamics are strongly coupled and highly nonlinear, it is necessary to compensate for these model features when designing accurate controllers. Furthermore, since AUVs often operate in harsh environments, the control laws need to be robust against unmodelled dynamics, model uncertainties, and external disturbance due to ocean currents.
Multiple nonlinear control schemes exist and a lot of literature is written on the subject. [44] is a comprehensive study of nonlinear modeling and control of small underwater vehicles. The thesis presented control schemes using feedback linearization, passivity, and sliding mode, as well as the combination of these.
SMC is a non-linear control law explained in detail in [45]. Since the primary function of each of the feedback channels is to switch between two distinctively different system structures to manifold a new type of system motion, the SMC is claimed to have superb system performance. This includes insensitivity to parameter variations and rejection of

disturbances [46]. These characteristics make it robust, hence a suitable option for AUV control. Control of AUVs using SMC is well documented, both for control in a decoupled horizontal/vertical plane [47] [48] and in 6 DOF [49] [44]. By defining sliding surfaces expressed in terms of the error signals for surge, sway, heave, roll, pitch, and yaw motion, zero tracking error in all DOFs can be achieved. Global stability can be ensured by applying Barbalat's Lyapunov-like lemma [50]. The literature validates the SMCs ability to track a desired trajectory and robustness against bounded disturbances and uncertain parameters.

When bounds of uncertainty are not known *a priori*, an adaptive approach might be needed to deal with the uncertainties. In [51] the performance of the adaptive control laws proposed by [37], referred to as ASB, and [36], referred to as DCAL, is discussed. What differs from the two schemes is that ASB uses the actual states as input in the parameterization and the virtual reference trajectories as input in the control law and parameter adaptation law, while DCAL uses the desired state as input for all three. The article stated that for perfect measurements the performance of both laws performs good and is almost identical. When introducing measurement noise it led to parameter drift when using ASB, while DCAL still performed satisfactorily. Since it is normal for an underwater vehicle to obtain its body-fixed velocities using a model-based state estimation through noisy position measurements, the authors concluded that DCAL is the superior control scheme for real-time AUV applications.

An adaptive sliding mode control (ASMC) law utilizes the adaptiveness of a direct adaptive method with the robustness of a sliding mode controller [48]. The presented ASMC in [50] consisted of a switching term compensating for the uncertainty in the input matrix and an on-line parameter estimation algorithm. The result was robust motion control in 6 DOF where environmental disturbances are compensated for.

[52] showed that adaptive extensions of sliding control are effective for precise control of underwater vehicles. The control scheme presented in the paper utilizes the intrinsic modeling performance tradeoff to determine when the current model of the system to be controlled is inadequate.

One problem with the SMC is the chattering that can occur from the switching term. In [44] this was dealt with by smoothing out the control law discontinuity inside a boundary layer, leading to a lowpass filter structure of the dynamics of the sliding surface.

Chapter 3

Theory and implementation

This chapter presents the general theory behind the 6 DOF E.O.M for an AUV and the sliding mode methodology, in sections 3.1 and 3.2, respectfully. Further, in section 3.3 the Simulink simulator of the REMUS 100 AUV, based on the general theory, is described and discussed. Lastly, the creation of a DT using CSE is presented in section 3.4.

3.1 Mathematical modeling

Using Fossen notation [17], the dynamics, including the kinematics and kinetics, in 6 DOF can be expressed in the following matrix form:

$$\dot{\boldsymbol{\eta}} = \boldsymbol{J}(\boldsymbol{\eta})\boldsymbol{\nu_r} \tag{3.1}$$

$$\boldsymbol{M}\dot{\boldsymbol{\nu}}_{\boldsymbol{r}} + \boldsymbol{C}\left(\boldsymbol{\nu}_{\boldsymbol{r}}\right)\boldsymbol{\nu}_{\boldsymbol{r}} + \boldsymbol{D}\left(\boldsymbol{\nu}_{\boldsymbol{r}}\right)\boldsymbol{\nu}_{\boldsymbol{r}} + \boldsymbol{g}(\boldsymbol{\eta}) + \boldsymbol{g}_o = \boldsymbol{\tau}. \tag{3.2}$$

In section 3.1.1 the kinematics presented in eq. (3.1) will be discussed, while in section 3.1.2 the kinetics given in eq. (3.2) is outlined.

3.1.1 Kinematics

Generally, an underwater vehicle model can be written with respect to either *NED-frame* or *BODY-frame*, as indicated in figure 3.1. The transformation matrix J, seen in equation 3.1, describes the transformation between the two frames and is given as

$$\boldsymbol{J} = \begin{bmatrix} \boldsymbol{R}\left(\boldsymbol{\Theta}_{nb}\right) & \mathbf{0}_{3\times 3} \\ \mathbf{0}_{3\times 3} & \boldsymbol{T}\left(\boldsymbol{\Theta}_{nb}\right) \end{bmatrix}. \tag{3.3}$$

where

$$\boldsymbol{R}\left(\boldsymbol{\Theta}_{nb}\right) = \begin{bmatrix} c\psi c\theta & -s\psi \mathbf{c}\phi + c\psi \mathbf{s}\theta s\phi & \mathbf{s}\psi \mathbf{s}\phi + c\psi c\phi s\theta \\ s\psi c\theta & c\psi c\phi + s\phi s\theta s\psi & -c\psi s\phi + s\theta s\psi c\phi \\ -s\theta & c\theta s\phi & c\theta c\phi \end{bmatrix} \tag{3.4}$$

and

$$\boldsymbol{T}(\boldsymbol{\Theta}_{nb}) = \begin{bmatrix} 1 & \mathrm{s}\phi\mathrm{t}\theta & \mathrm{c}\phi\mathrm{t}\theta \\ 0 & \mathrm{c}\phi & -\mathrm{s}\phi \\ 0 & \mathrm{s}\phi/\mathrm{c}\theta & \mathrm{c}\phi/\mathrm{c}\theta \end{bmatrix}. \tag{3.5}$$

In equation 3.4 and 3.5, c, s and t, represent $cos(.)$, $sin(.)$ and $tan(.)$, respectively. The major problem with this representation using Euler angles is the singularity issue when $\theta = 90°$. An alternative is using unit quaternions, which is a four-parameter method without singularity problems [17].
Moreover, $\boldsymbol{\eta} = [x, y, z, \phi, \theta, \psi]^\top$ and $\boldsymbol{\nu_r} = \boldsymbol{\nu} - \boldsymbol{\nu_c} = [u - u_c, v - v_c, w - w_c, p, q, r]^\top = [u_r, v_r, w_r, p, q, r]^\top$. Here $\boldsymbol{\eta}$ denotes the position and orientation of the vehicle relative to *NED-frame*, while $\boldsymbol{\nu_r}$ represents the velocities and angular rates relative to *BODY-frame*. Table 3.1 summarizes the notation.

DOF		Forces and moments	Linear and angular velocities	Positions and Euler angles
1	motions in the x -direction (surge)	X	u	x
2	motions in the y -direction (sway)	Y	v	y
3	motions in the z -direction (heave)	Z	w	z
4	rotation about the x -axis (roll)	K	p	ϕ
5	rotation about the y -axis (pitch)	M	q	θ
6	rotation about the z -axis (yaw)	N	r	ψ

Table 3.1: Notation for marine vessels

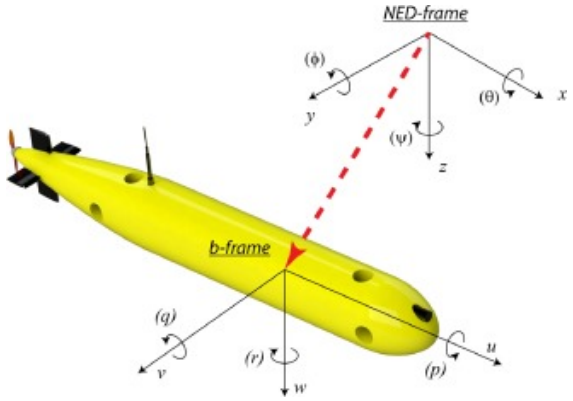

Figure 3.1: AUV *NED-frame* and *NED-frame*

3.1.2 Kinetics

The system inertia matrix, $\boldsymbol{M}$, and the Coriolis-centripetal matrix, $\boldsymbol{C}(\boldsymbol{\nu_r})$ is given as

$$\begin{aligned} \boldsymbol{M} &= \boldsymbol{M}_{RB} + \boldsymbol{M}_{A} \\ \boldsymbol{C}\left(\boldsymbol{\nu}_r\right) &= \boldsymbol{C}_{RB}\left(\boldsymbol{\nu}_r\right) + \boldsymbol{C}_{A}\left(\boldsymbol{\nu}_r\right) \end{aligned} \tag{3.6}$$

where the notations $\boldsymbol{RB}$ and $\boldsymbol{A}$ stands for matrices caused by rigid body and added mass, respectively. For an underwater vehicle, starboard-port symmetry is common, resulting in $y_g = I_{xy} = I_{yz} = 0$ [17]. The system inertia matrix can then be written as:

$$\boldsymbol{M} = \begin{bmatrix} m - X_{\dot{u}} & 0 & -X_{\dot{w}} & 0 & mz_g - X_{\dot{q}} & 0 \\ 0 & m - Y_{\dot{v}} & 0 & -mz_g - Y_{\dot{p}} & 0 & mx_g - Y_{\dot{r}} \\ -X_{\dot{w}} & 0 & m - Z_{\dot{w}} & 0 & -mx_g - Z_{\dot{q}} & 0 \\ 0 & -mz_g - Y_{\dot{p}} & 0 & I_x - K_{\dot{p}} & 0 & -I_{zx} - K_{\dot{r}} \\ mz_g - X_{\dot{q}} & 0 & -mx_g - Z_{\dot{q}} & 0 & I_y - M_{\dot{q}} & 0 \\ 0 & mx_g - Y_{\dot{r}} & 0 & -I_{zx} - K_{\dot{r}} & 0 & I_z - N_{\dot{r}} \end{bmatrix} \tag{3.7}$$

where m denotes the rigid body mass of the AUV and $\boldsymbol{r_g} = [x_g, y_g, z_g]^T$ the center of gravity. I_x, I_y and I_z are the moments of interia, and I_{zx}, I_{xy} and I_{yz} are the products of inertia. Moreover, X_i, Y_i, Z_i, K_i, M_i and N_i, where $i = \dot{u}, \dot{v}, \dot{w}, \dot{p}, \dot{q}, \dot{r}$, represent the added mass terms.
Further, following theorem 3.2 of Fossen [17], it is stated that the rigid-body Coriolis-centripetal matrix $\boldsymbol{C_{RB}(\nu)}$ can always be represented such that it is skew-symmetric. This implies that the quadratic form $\boldsymbol{\nu}^T \boldsymbol{C_{RB}(\nu)\nu} = 0$, making the skew-symmetric property very useful when designing a nonlinear motion control system. The added mass Coriolis-centripetal matrix $\boldsymbol{C_A(\nu)}$ for an AUV moving in 6 DOF will in the general case be highly nonlinear and coupled.

The highly coupled and nonlinear damping matrix, $\boldsymbol{D(\nu_r)}$, can be described mathematically as:

$$\boldsymbol{D}_n\left(\boldsymbol{\nu}_r\right)\boldsymbol{\nu}_r = \begin{bmatrix} |\boldsymbol{\nu}_r|^\top \boldsymbol{D}_{n1}\boldsymbol{\nu}_r \\ |\boldsymbol{\nu}_r|^\top \boldsymbol{D}_{n2}\boldsymbol{\nu}_r \\ |\boldsymbol{\nu}_r|^\top \boldsymbol{D}_{n3}\boldsymbol{\nu}_r \\ |\boldsymbol{\nu}_r|^\top \boldsymbol{D}_{n4}\boldsymbol{\nu}_r \\ \boldsymbol{\nu}_r|^\top \boldsymbol{D}_{n4}\boldsymbol{\nu}_r \\ \boldsymbol{V}_r|^\top \boldsymbol{D}_{n6}\boldsymbol{\nu}_r \end{bmatrix} \tag{3.8}$$

where $\boldsymbol{D_{ni}}\left(\boldsymbol{\nu_r}\right)$ for $i = 1, \ldots, 6$ is $6x6$ matrices.
The submerged weight of the body and buoyancy forces for, $\boldsymbol{g(\eta)}$, can be modeled as

$$\boldsymbol{g}(\boldsymbol{\eta}) = \begin{bmatrix} (W-B)\sin(\theta) \\ -(W-B)\cos(\theta)\sin(\phi) \\ -(W-B)\cos(\theta)\cos(\phi) \\ -(y_g W - y_b B)\cos(\theta)\cos(\phi) + (z_g W - z_b B)\cos(\theta)\sin(\phi) \\ (z_g W - z_b B)\sin(\theta) + (x_g W - x_b B)\cos(\theta)\sin(\phi) \\ -(x_g W - x_b B)\cos(\theta)\sin(\phi) - (y_g W - y_b B)\sin(\theta) \end{bmatrix}. \tag{3.9}$$

Here $W = mg$ denotes the gravitational force acting through the CG and $B = \rho g \Delta$ the buoyancy force acting through the CB. Both the CG and the CB are defined relativel to the CO by the vectors $\boldsymbol{r_g^b} = [x_g, y_g, z_g]^T$ and $\boldsymbol{r_b^b} = [x_b, y_b, z_b]^T$, respectively. Static restoring forces and moments due to ballast systems and water tanks are collected in the term g_0.
Since the effects of wind and waves are neglectable when at a certain depth, $\boldsymbol{\tau}$ will only consist of forces and moments caused by the actuators and the current. It is given as

$$\boldsymbol{\tau} = \begin{bmatrix} \sum X \\ \sum Y \\ \sum Z \\ \sum K \\ \sum M \\ \sum N \end{bmatrix} \tag{3.10}$$

where X, Y, Z are forces in surge, sway and heave, respectively, and K, M, N are moments in roll, pitch and yaw, respectively.

The kinetics will be quite complicated in the general case. However, it is shown in section 3.3 how the complexity can be reduced using body-symmetry conditions and neglecting highly non-linear coupling terms.

3.2 Sliding Mode Control

The dynamics of underwater vehicles present a difficult control system design that traditional linear design methods cannot accommodate easily [45]. SMC is a nonlinear design technique that can deal with nonlinear dynamics directly and is shown to be stable despite errors in hydrodynamic coefficients and unmodelled disturbances. Using a dynamic model of the system combined with a sliding surface definition we can use Lyaponovs stability criteria to derive a suitable control law.

For a tracking controller, which is often the case for an AUV, the control problem is to make the state, $\boldsymbol{x}$, follow a prescribed state, $\boldsymbol{x_d}$. The tracking error is defined as:

$$\tilde{\boldsymbol{x}} = \boldsymbol{x} - \boldsymbol{x_d} \tag{3.11}$$

The next step is to define a time-varying sliding surface, $\boldsymbol{s}$, so that $\tilde{\boldsymbol{x}} \to 0$ as $t \to \infty$. The simplest function satisfying this criterion is:

$$\boldsymbol{s}(\boldsymbol{x};\boldsymbol{t}) := \dot{\tilde{\boldsymbol{x}}} + \lambda\tilde{\boldsymbol{x}} \tag{3.12}$$

where $\lambda > 0$ is a design parameter reflecting the bandwidth of the controller [17].Consequently, if $\boldsymbol{s}$ is driven to zero, the tracking error will also be driven to zero. A Lyapunov-like function is then considered, such as:

$$\boldsymbol{V}(\boldsymbol{s}) = \frac{1}{2}\boldsymbol{s}^2. \tag{3.13}$$

Differentiation $\boldsymbol{V}$ with respect to the sliding surface yields:

$$\dot{\boldsymbol{V}}(\boldsymbol{s}) = \boldsymbol{s}\dot{\boldsymbol{s}} = \boldsymbol{s}[\ddot{\tilde{\boldsymbol{x}}} + \lambda\dot{\tilde{\boldsymbol{x}}}]. \tag{3.14}$$

The relation between the dynamic model of the system and the sliding surface, $\boldsymbol{s}$, is then used to derive a control law so that $\dot{\boldsymbol{V}} < 0$ for all $\boldsymbol{s} \neq 0$. This ensures exponential stability of $\boldsymbol{s} = 0$, leading the sliding manifold to converge to zero and in return making $\tilde{\boldsymbol{x}} \to 0$ in finite time.

3.3 Simulation Environment

To perform a simulation study of the SMC algorithm, a simulator using Simulink and MATLAB was built. The simulator is divided into three major parts; the AUV model, the SMC controller and the guidance system, all of which are elaborated in sections 3.3.1 to 3.3.3, respectfully. The high level structure of subsystems and the connections between them is presented in fig. 3.2.

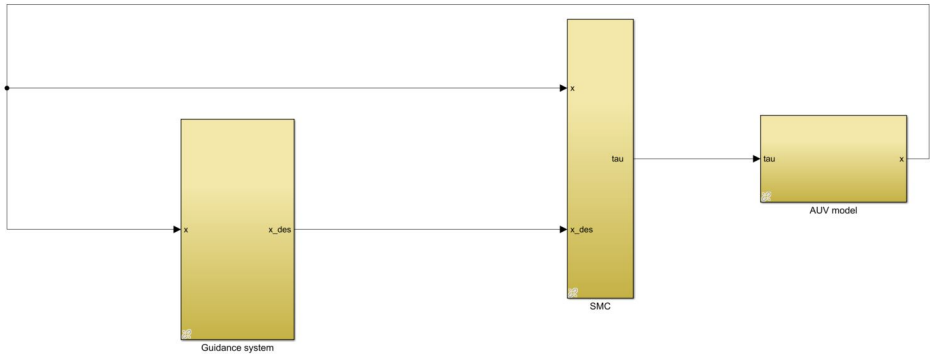

Figure 3.2: High level structure of AUV simulator

3.3.1 AUV model

Since the scope of this study is the control algorithm, a simulator created by Petter Norgren [53] and based on the work of Timothy Prestero [20], was used to describe the AUV dynamics. Figure 3.3 shows the AUV model in Simulink.

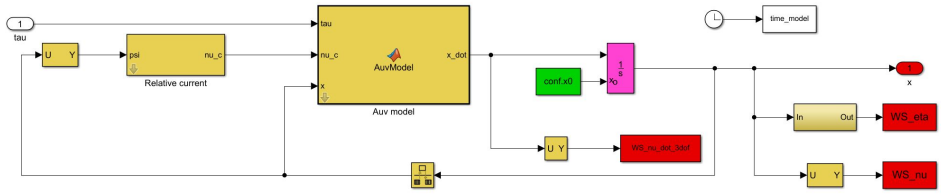

Figure 3.3: AUV model

The *AuvModel* block describes the dynamics and kinetics of the AUV, which can be written mathematically as:

$$\dot{\boldsymbol{\eta}} = \boldsymbol{J}(\boldsymbol{\eta})\boldsymbol{\nu} \tag{3.15}$$

$$\boldsymbol{M}\dot{\boldsymbol{\nu}} + \boldsymbol{C_{RB}}(\boldsymbol{\nu})\boldsymbol{\nu} + \boldsymbol{C_A}(\boldsymbol{\nu_r})\boldsymbol{\nu_r} + \boldsymbol{D}(\boldsymbol{\nu_r})\boldsymbol{\nu_r} + \boldsymbol{g}(\boldsymbol{\eta}) = \boldsymbol{\tau}. \tag{3.16}$$

Equations (3.15) and (3.16) are results of the study of Prestero, suggesting that $\boldsymbol{C_{RB}}$ is no longer dependent on $\boldsymbol{\nu_r}$. Further, since the products of inertia are small compared to the moments of inertia, they are assumed to be zero, in effect assuming that the AUV has post/starboard and top/bottom symmetry. As a result, the the system inertia matrix, $\boldsymbol{M}$, is found to be:

$$\boldsymbol{M} = \begin{bmatrix} 31.4091 & 0 & 0 & 0 & .5974 & 0 \\ 0 & 65.9791 & 0 & -0.5974 & 0 & -1.9300 \\ 0 & 0 & 65.9791 & 0 & 1.9300 & 0 \\ 0 & -0.5974 & 0 & 0.2591 & 0 & 0 \\ 0.5974 & 0 & 1.9300 & 0 & 8.3417 & 0 \\ 0 & -1.9300 & 0 & 0 & 0 & 8.3300 \end{bmatrix} kg. \tag{3.17}$$

Assuming only low-speed operations combined with the symmetric properties of the REMUS 100, the added mass Coriolis-centripetal matrix is simplified into a skew-symmetric matrix given as

$$\boldsymbol{C_A}\left(\boldsymbol{\nu_r}\right) = -\boldsymbol{C_A^\top}\left(\boldsymbol{\nu_r}\right) = \begin{bmatrix} 0 & 0 & 0 & 0 & -Z_{\dot{w}}w & Y_{\dot{v}}v_r \\ 0 & 0 & 0 & Z_{\dot{w}}w & 0 & -X_{\dot{u}}u_r \\ 0 & 0 & 0 & -Y_{\dot{v}}v_r & X_{\dot{u}}u_r & 0 \\ 0 & -Z_{\dot{w}}w & Y_{\dot{v}}v_r & 0 & -N_{\dot{r}}r & M_{\dot{q}}q \\ Z_{\dot{w}}w & 0 & -X_{\dot{u}}u_r & N_{\dot{r}}r & 0 & -K_{\dot{p}}p \\ -Y_{\dot{v}}v_r & X_{\dot{u}}u_r & 0 & -M_{\dot{q}}q & K_{\dot{p}}p & 0 \end{bmatrix}. \tag{3.18}$$

Additionally, linear and angular coupled damping terms, as well as damping terms greater than second order, are neglected. The resulting damping matrix is modeled as

$$\boldsymbol{D}\left(\boldsymbol{\nu_r}\right) = \begin{bmatrix} X_{uu}|u_r| & 0 & 0 & 0 & 0 & 0 \\ 0 & Y_{vv}|v_r| & 0 & 0 & 0 & -Y_{rr}|r| \\ 0 & 0 & Z_{ww}|w| & 0 & -Z_{qq}|q| & 0 \\ 0 & 0 & 0 & K_{pp}|p| & 0 & 0 \\ 0 & 0 & -M_{ww}|w| & 0 & M_{qq}|q| & 0 \\ 0 & -N_{vv}|v| & 0 & 0 & 0 & N_{rr}|r| \end{bmatrix}. \tag{3.19}$$

The values of the numerical coefficients can be viewed in appendix A. Moreover, the center of buoyancy (CB) and the center of gravity (CG) is described by the following vectors

$$\boldsymbol{r_g^b} = \begin{bmatrix} 0 \\ 0 \\ 0.0196 \end{bmatrix} \quad \boldsymbol{r_b^b} = \begin{bmatrix} 0 \\ 0 \\ 0 \end{bmatrix}, \tag{3.20}$$

thus the submerged weight of the body and buoyancy forces are

$$\boldsymbol{g}(\boldsymbol{\eta}) = \begin{bmatrix} (W-B)\sin(\theta) \\ -(W-B)\cos(\theta)\sin(\phi) \\ -(W-B)\cos(\theta)\cos(\phi) \\ z_g W\cos(\theta)\sin(\phi) \\ z_g W\sin(\theta) \\ 0 \end{bmatrix}. \tag{3.21}$$

The current is modeled with a direction and velocity in *NED-frame*, resulting in ν_c, which represent the current relative to the AUV body, is given as $[u_r, v_r, 0, 0, 0, 0]^T$.

3.3.2 Sliding Mode Control of the REMUS 100

In this , the robust SMC designed for the REMUS 100 AUV simulator is elaborated. The objective of the controller is to make the tracking error converge to zero in the presence of environmental disturbances and parameter uncertainties. Figure 3.4 shows the designed SMC where *x* and *x_des* denote the actual and desired state, respectfully, and *tau* is the force calculated by the *sliding_mode* MATLAB code. The state is given as $[\boldsymbol{\eta} \quad \boldsymbol{\nu}]^T$.

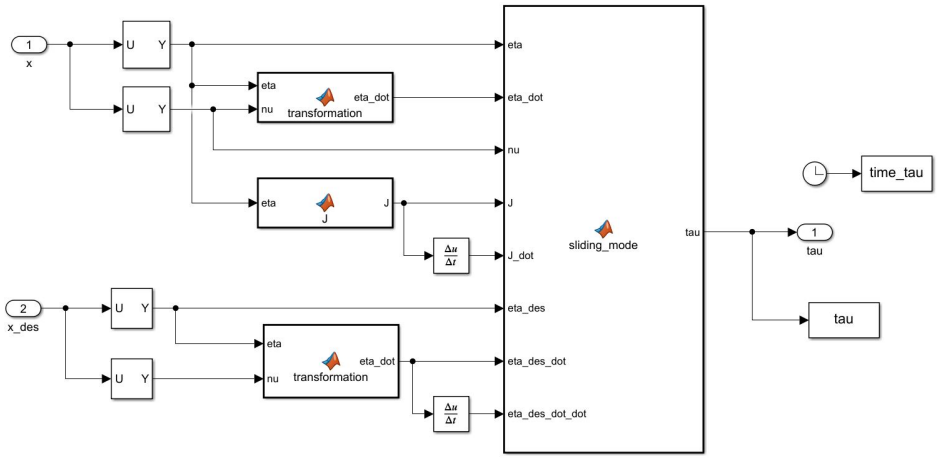

Figure 3.4: Sliding mode controller

The first step of the design process is to reorganize the AUV dynamics described in 3.3.1 and rewrite equation 3.16 and 3.15 into:

$$\dot{\boldsymbol{\eta}} = \boldsymbol{J}(\boldsymbol{\eta})\boldsymbol{\nu} \tag{3.22}$$

$$\boldsymbol{M}\dot{\boldsymbol{\nu}} = \boldsymbol{\tau} - \boldsymbol{C_{RB}}(\boldsymbol{\nu})\boldsymbol{\nu} - \boldsymbol{C_A}(\boldsymbol{\nu_r})\boldsymbol{\nu_r} - \boldsymbol{D}(\boldsymbol{\nu_r})\boldsymbol{\nu_r} - \boldsymbol{g}(\boldsymbol{\eta}). \tag{3.23}$$

Further, the following relationship:

$$\ddot{\boldsymbol{\eta}} = \boldsymbol{J}(\boldsymbol{\eta})\dot{\boldsymbol{\nu}} + \dot{\boldsymbol{J}}(\boldsymbol{\eta})\boldsymbol{\nu} \Rightarrow \dot{\boldsymbol{\nu}} = \boldsymbol{J}(\boldsymbol{\eta})^{-1}(\ddot{\boldsymbol{\eta}} - \dot{\boldsymbol{J}}(\boldsymbol{\eta})\boldsymbol{J}(\boldsymbol{\eta})^{-1}\dot{\boldsymbol{\eta}}) \tag{3.24}$$

is used to represent 3.23 in *NED-frame*:

$$\ddot{\boldsymbol{\eta}} = \boldsymbol{M}^{*-1}(\boldsymbol{\tau}^* - \boldsymbol{C}^*_{\boldsymbol{RB}}\dot{\boldsymbol{\eta}} - \boldsymbol{C}^*_{\boldsymbol{A}}\dot{\boldsymbol{\eta}}_{\boldsymbol{r}} - \boldsymbol{D}^*\dot{\boldsymbol{\eta}}_{\boldsymbol{r}} - \boldsymbol{g}^*) \tag{3.25}$$

where

$$\boldsymbol{M}^* = \boldsymbol{J}^{-\boldsymbol{T}}(\boldsymbol{\eta})\boldsymbol{M}\boldsymbol{J}^{-\boldsymbol{1}}(\boldsymbol{\eta}) \tag{3.26}$$

$$\boldsymbol{C}^*_{\boldsymbol{RB}} = \boldsymbol{J}^{-\boldsymbol{T}}(\boldsymbol{\eta})[\boldsymbol{C_{RB}}(\boldsymbol{\nu}) - \boldsymbol{M}\boldsymbol{J}^{-\boldsymbol{1}}(\boldsymbol{\eta})\dot{\boldsymbol{J}}(\boldsymbol{\eta})]\boldsymbol{J}^{-\boldsymbol{1}}(\boldsymbol{\eta}) \tag{3.27}$$

$$\boldsymbol{C}^*_{\boldsymbol{A}} = \boldsymbol{J}^{-\boldsymbol{T}}(\boldsymbol{\eta})\boldsymbol{C_A}(\boldsymbol{\nu_r})\boldsymbol{J}^{-\boldsymbol{1}}(\boldsymbol{\eta}) \tag{3.28}$$

$$\boldsymbol{D}^* = \boldsymbol{J}^{-\boldsymbol{T}}(\boldsymbol{\eta})\boldsymbol{D}(\boldsymbol{\nu_r})\boldsymbol{J}^{-\boldsymbol{1}}(\boldsymbol{\eta}) \tag{3.29}$$

$$\boldsymbol{g}^* = \boldsymbol{J}^{-\boldsymbol{T}}(\boldsymbol{\eta})\boldsymbol{g}(\boldsymbol{\eta}) \tag{3.30}$$

$$\boldsymbol{\tau}^* = \boldsymbol{J}^{-\boldsymbol{T}}(\boldsymbol{\eta})\boldsymbol{\tau}. \tag{3.31}$$

$$\tag{3.32}$$

Since $\boldsymbol{M} = \boldsymbol{M}^T > 0$ and $\boldsymbol{D} > 0 \quad \forall \boldsymbol{\nu}$, it implies that also $\boldsymbol{M^*} = \left(\boldsymbol{M^*}\right)^T > 0$ and $\boldsymbol{D^*} > 0$ [17].

The current is neglected when designing the control law, thus making $\boldsymbol{\nu_r} = \boldsymbol{\nu}$ and $\boldsymbol{\eta_r} = \boldsymbol{\eta}$ in eq. (3.25). For simplicity, the rigid body and added mass centripetal and Coriolis matrices, $\boldsymbol{C^*_{RB}}$ and $\boldsymbol{C^*_A}$, are added together and presented as $\boldsymbol{C^*}$:

$$\begin{aligned}
\boldsymbol{C^*} &= \boldsymbol{C^*_{RB}} + \boldsymbol{C^*_A} && (3.33)\\
&= \boldsymbol{J^{-T}}(\boldsymbol{\eta})[\boldsymbol{C_{RB}}(\boldsymbol{\nu}) + \boldsymbol{C_A}(\boldsymbol{\nu}) - \boldsymbol{M}\boldsymbol{J^{-1}}(\boldsymbol{\eta})\dot{\boldsymbol{J}}(\boldsymbol{\eta})]\boldsymbol{J^{-1}}(\boldsymbol{\eta}) && (3.34)\\
&= \boldsymbol{J^{-T}}(\boldsymbol{\eta})[\boldsymbol{C}(\boldsymbol{\nu}) - \boldsymbol{M}\boldsymbol{J^{-1}}(\boldsymbol{\eta})\dot{\boldsymbol{J}}(\boldsymbol{\eta})]\boldsymbol{J^{-1}}(\boldsymbol{\eta}). && (3.35)
\end{aligned}$$

Combining this, $\ddot{\boldsymbol{\eta}}$ can be written as:

$$\ddot{\boldsymbol{\eta}} = \boldsymbol{M^{*-1}}(\boldsymbol{\tau^*} - \boldsymbol{C^*}\dot{\boldsymbol{\eta}} - \boldsymbol{D^*}\dot{\boldsymbol{\eta}} - \boldsymbol{g^*}) \tag{3.36}$$

As in 3.3.2, the defined sliding surface is

$$\boldsymbol{s} := \dot{\tilde{\boldsymbol{\eta}}} + \lambda\tilde{\boldsymbol{\eta}}, \tag{3.37}$$

where $\tilde{\boldsymbol{\eta}} = \boldsymbol{\eta} - \boldsymbol{\eta_d}$ is the tracking error and λ is the control bandwith. For $\boldsymbol{s} = 0$, eq. (3.37) describes a sliding surface, or manifold, with exponentially stable dynamics, thus resulting in $\tilde{\boldsymbol{\eta}}$ converging exponentially to zero.

Further, for convenience, a viritual reference $\boldsymbol{\eta_v}$ is defined to satisfy

$$\dot{\boldsymbol{\eta_v}} := \dot{\boldsymbol{\eta_d}} - \lambda\tilde{\boldsymbol{\eta}} \Rightarrow s := \dot{\boldsymbol{\eta}} - \dot{\boldsymbol{\eta_v}}, \tag{3.38}$$

which results in

$$\dot{\boldsymbol{s}} := \ddot{\boldsymbol{\eta}} - \ddot{\boldsymbol{\eta_v}}. \tag{3.39}$$

A Lyaponov-like function candidate is then considered:

$$\boldsymbol{V}(\boldsymbol{s}, \boldsymbol{t}) = \frac{1}{2}\boldsymbol{s^T}\boldsymbol{M^*}\boldsymbol{s}. \tag{3.40}$$

Differentiating V with respect to time yields

$$\begin{aligned}
\dot{\boldsymbol{V}} &= \frac{\mathbf{1}}{\mathbf{2}}\boldsymbol{s^T}\dot{\boldsymbol{M}}^*\boldsymbol{s} + \boldsymbol{s^T}\boldsymbol{M^*}\dot{\boldsymbol{s}} - \boldsymbol{s^T}\boldsymbol{C^*}\boldsymbol{s} + \boldsymbol{s^T}\boldsymbol{C^*}\boldsymbol{s} && (3.41)\\
&= \boldsymbol{s^T}\boldsymbol{M^*}\dot{\boldsymbol{s}} + \frac{\mathbf{1}}{\mathbf{2}}\boldsymbol{s^T}(\dot{\boldsymbol{M}}^* - \mathbf{2}\boldsymbol{C^*})\boldsymbol{s} + \boldsymbol{s^T}\boldsymbol{C^*}\boldsymbol{s}. && (3.42)
\end{aligned}$$

Using the relations found in eq. (3.26) and eq. (3.27), $\dot{\boldsymbol{M}}^*$ can be written as

$$\dot{\boldsymbol{M}}^* = \boldsymbol{J}^{-T}(\boldsymbol{\eta})(\dot{\boldsymbol{M}} - 2\boldsymbol{M}\boldsymbol{J}^{-1}(\boldsymbol{\eta})\dot{\boldsymbol{J}}(\boldsymbol{\eta}))\boldsymbol{J}^{-1}(\boldsymbol{\eta}) \tag{3.43}$$

$$= \boldsymbol{J}^{-T}(\boldsymbol{\eta})(\dot{\boldsymbol{M}} - 2([\boldsymbol{C} - \boldsymbol{J}^{T}(\boldsymbol{\eta})\boldsymbol{C}^*\boldsymbol{J}(\boldsymbol{\eta})]\boldsymbol{J}(\boldsymbol{\eta})\dot{\boldsymbol{J}}^{-1}(\boldsymbol{\eta}))). \tag{3.44}$$

Moreover, eq. (3.44) can be presented as:

$$\dot{\boldsymbol{M}}^* - \boldsymbol{2C}^* = \boldsymbol{J}^{-T}(\boldsymbol{\eta})(\dot{\boldsymbol{M}} - \boldsymbol{2C})\boldsymbol{J}^{-1}(\boldsymbol{\eta}). \tag{3.45}$$

Since $\dot{\boldsymbol{M}} - 2\boldsymbol{C}$ is skew-symmetric it follows that $\dot{\boldsymbol{M}}^* - 2\boldsymbol{C}^*$ is skew-symmetric as well.

Applying the skew-symmetric property $\boldsymbol{s}^{\boldsymbol{T}}(\dot{\boldsymbol{M}}^* - 2\boldsymbol{C}^*)\boldsymbol{s} = 0, \forall \boldsymbol{s}$ reduces $\dot{\boldsymbol{V}}$ into

$$\dot{\boldsymbol{V}} = \boldsymbol{s}^{\boldsymbol{T}}\boldsymbol{M}^*\dot{\boldsymbol{s}} + \boldsymbol{s}^{\boldsymbol{T}}\boldsymbol{C}^*\boldsymbol{s}. \tag{3.46}$$

By substituting $\ddot{\boldsymbol{\eta}}$ from eq. (3.25) and using the relation $\dot{\boldsymbol{\eta}} := \boldsymbol{s} + \boldsymbol{\eta}_{\boldsymbol{v}}$ from eq. (3.37) it can be shown that:

$$\dot{\boldsymbol{V}} = -\boldsymbol{s}^{\boldsymbol{T}}\boldsymbol{D}^*\boldsymbol{s} + \boldsymbol{s}^{\boldsymbol{T}}(\boldsymbol{\tau}^* - \boldsymbol{M}^*\dot{\boldsymbol{\nu}}_{\boldsymbol{v}} - \boldsymbol{C}^*\dot{\boldsymbol{\nu}}_{\boldsymbol{v}} - \boldsymbol{D}^*\boldsymbol{\nu}_{\boldsymbol{v}} - \boldsymbol{g}^*). \tag{3.47}$$

Choosing the control law to be

$$\boldsymbol{\tau}^* = \boldsymbol{M}^*\ddot{\boldsymbol{\eta}}_{\boldsymbol{v}} + \hat{\boldsymbol{C}}^*\dot{\boldsymbol{\eta}}_{\boldsymbol{v}} + \hat{\boldsymbol{D}}^*\dot{\boldsymbol{\eta}}_{\boldsymbol{v}} + \boldsymbol{g}^* - \boldsymbol{K}_{\boldsymbol{d}}\boldsymbol{s} - \boldsymbol{K}_{\boldsymbol{s}}\boldsymbol{sgn}(\boldsymbol{s}) \tag{3.48}$$

$$= \boldsymbol{M}^*\ddot{\boldsymbol{\eta}}_{\boldsymbol{v}} + \boldsymbol{C}^*_{\boldsymbol{RB}}\dot{\boldsymbol{\eta}}_{\boldsymbol{v}} + \hat{\boldsymbol{C}}^*_{\boldsymbol{A}}\dot{\boldsymbol{\eta}}_{\boldsymbol{v}} + \hat{\boldsymbol{D}}^*\dot{\boldsymbol{\eta}}_{\boldsymbol{v}} + \boldsymbol{g}^* - \boldsymbol{K}_{\boldsymbol{d}}\boldsymbol{s} - \boldsymbol{K}_{\boldsymbol{s}}\boldsymbol{sgn}(\boldsymbol{s}) \tag{3.49}$$

where $\hat{\boldsymbol{C}}^*_{\boldsymbol{A}}$ and $\hat{\boldsymbol{D}}^*$ denotes the estimates of $\boldsymbol{C}^*_{\boldsymbol{A}}$ and $\boldsymbol{D}^*$, due to unknown current, it follows that

$$\dot{\boldsymbol{V}} = -\boldsymbol{s}^{\boldsymbol{T}}(\boldsymbol{D}^* + \boldsymbol{K}_{\boldsymbol{d}})\boldsymbol{s} + \boldsymbol{s}^{\boldsymbol{T}}(\tilde{\boldsymbol{C}_{\boldsymbol{A}}}\dot{\boldsymbol{\nu}}_{\boldsymbol{v}} + \tilde{\boldsymbol{D}}\dot{\boldsymbol{\nu}}_{\boldsymbol{v}}) - \boldsymbol{K}_{\boldsymbol{s}}|\boldsymbol{s}|. \tag{3.50}$$

$\tilde{\boldsymbol{C}^*_{\boldsymbol{A}}} = \hat{\boldsymbol{C}}^*_{\boldsymbol{A}} - \boldsymbol{C}^*_{\boldsymbol{A}}$ and $\tilde{\boldsymbol{D}}^* = \hat{\boldsymbol{D}}^* - \boldsymbol{D}^*$ represent the parameter error of the model.

Chattering is a phenomenon causing undesirable oscillations with finite amplitude and frequency due to unmodeled dynamics and may cause decreased control performance and wear of actuators [54]. To avoid chattering, [55] propose to choose $\boldsymbol{sgn}(\boldsymbol{s})$ as

$$\mathrm{sgn}_i(s_i/\phi) = \begin{cases} 1 & \text{if} \quad \frac{s_i}{\phi} > 1 \\ s_i/\phi & \text{if} \quad -1 \leq \frac{s_i}{\phi} \leq 1 \\ -1 & \text{if} \quad \frac{s_i}{\phi} < -1 \end{cases} \tag{3.51}$$

to smooth out the discontinuity inside a boundary layer and assign a low pass filter structure to the dynamics of the sliding surface [44]. In eq. (3.51), i represent each DOF, while $\phi < 0$ can be interpreted as the boundary layer thickness.

The switching gain vector, $\boldsymbol{K}_{\boldsymbol{s}}$, is found by requiring $\dot{\boldsymbol{V}} \leq 0$. Consequently, $\boldsymbol{K}_{\boldsymbol{s}}$ is chosen to satisfy:

$$\boldsymbol{K_s} \geq |\tilde{\boldsymbol{C}_{\boldsymbol{A}}^*}\dot{\boldsymbol{\eta}}_{\boldsymbol{v}} + \tilde{\boldsymbol{D}^*}\dot{\boldsymbol{\eta}}_{\boldsymbol{v}}| + \gamma \quad , \quad \gamma > 0 \tag{3.52}$$

which dominates the parameter errors and reduces $\dot{\boldsymbol{V}}$ into:

$$\dot{\boldsymbol{V}} = -\boldsymbol{s}^{\boldsymbol{T}}(\boldsymbol{D}^* + \boldsymbol{K_d})\boldsymbol{s} - \gamma|\boldsymbol{s}|, \tag{3.53}$$

implying that

$$\dot{\boldsymbol{V}} \leq 0. \tag{3.54}$$

As explained earlier the damping matrix $\boldsymbol{D} > 0 \Rightarrow \boldsymbol{D}^* > 0$, thus making the design parameter matrix $\boldsymbol{K_d} \geq 0$, which again implies that $(\boldsymbol{D}^* + \boldsymbol{K_d}) \geq 0$. Hence, s is bounded and $\dot{\boldsymbol{V}}$ is uniformly continuous. Barbalat's lemma (appendix B) therefore ensures that $\boldsymbol{s} \to 0$ and thus $\tilde{\boldsymbol{\eta}} \to 0$ as $t \to 0$ [44].

Tuning of parameters

By inspecting the designed control law in 3.48 we can separate it into three terms [44]:

- feed-forward term: $\boldsymbol{M}^*\ddot{\boldsymbol{\eta}}_{\boldsymbol{v}} + \hat{\boldsymbol{C}}^*\dot{\boldsymbol{\eta}}_{\boldsymbol{v}} + \hat{\boldsymbol{D}}^*\dot{\boldsymbol{\eta}}_{\boldsymbol{v}} + \boldsymbol{g}^*$
- proportional-derivative (PD) term: $-\boldsymbol{K_d}\boldsymbol{s}$
- robustness term: $-\boldsymbol{K_s}\boldsymbol{sgn}(\boldsymbol{s})$

Decent performance can be achieved by just tuning the PD term before adding the feed-forward term to the control law. The PD-term alone turns the SMC into a PD-controller. By trial and error $\boldsymbol{K_d}$ was found to be:

$$\boldsymbol{K_d} = \begin{bmatrix} 1500 & 0 & 0 & 0 & 0 & 0 \\ 0 & 3000 & 0 & 0 & 0 & 0 \\ 0 & 0 & 1000 & 0 & 0 & 0 \\ 0 & 0 & 0 & 20 & 0 & 0 \\ 0 & 0 & 0 & 0 & 1600 & 0 \\ 0 & 0 & 0 & 0 & 0 & 1550 \end{bmatrix} \tag{3.55}$$

.

For the robustness term, since $\tilde{\boldsymbol{C}_{\boldsymbol{A}}^*}$ and $\tilde{\boldsymbol{D}^*}$ is unknown, a normal approach is to assume a percentage model uncertainty, α, for the estimates:

$$\boldsymbol{K_s} = \alpha|\hat{\boldsymbol{C}_{\boldsymbol{A}}^*}\dot{\boldsymbol{\eta}}_{\boldsymbol{v}} + \hat{\boldsymbol{D}^*}\dot{\boldsymbol{\eta}}_{\boldsymbol{v}}|. \tag{3.56}$$

20 percent uncertainty ($\alpha = 0.2$) was found to yield good results.

The control bandwith, λ, and boundary layer thickness, ϕ, was found to be 1.8 and 0.35, respectfully.

3.3.3 Guidance system

In the guidance system, a predefined list of north, east and depth coordinates, $conf.trajectory$, is used together with the current state, **x**, to calculate the desired heading, chi_d. The reference system then uses the calculated heading and the desired depth, z_d, and speed in surge, $conf.Uref$, to calculate the desired state, **x_des**. Figure 3.5 shows the Simulink implementation.

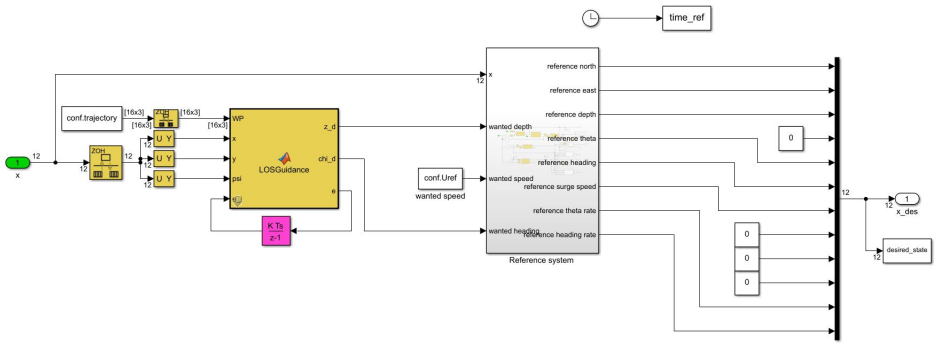

Figure 3.5: Guidance system

The *LOSGuidance* block was created by Petter Norgren [53] and the LOS algorithm is explained in detail in [17]. The reference model, found in the *Reference system* block, is used to force a smooth reference trajectory and not cause saturation for the control system. A third-order reference model, $\boldsymbol{\eta_r}$, was chosen for the positions (z_r and ψ_r), while one of second-order, $\boldsymbol{\nu_r}$, was used for the velocity (u_r). This suggests that a first-order low pass filter should be cascaded with a mass-damper-spring system, giving us the following vectorial expression for $\boldsymbol{\eta_r}$:

$$\boldsymbol{\eta_r} + (2\boldsymbol{\Delta} + \boldsymbol{I})\Omega\ddot{\boldsymbol{\eta}}_{\boldsymbol{r}} + (2\boldsymbol{\Delta} + \boldsymbol{I})\boldsymbol{\Omega^2}\dot{\boldsymbol{\eta}}_{\boldsymbol{r}} + \boldsymbol{\Omega^3}\boldsymbol{\eta_r} = \boldsymbol{\Omega^3}. \tag{3.57}$$

For the second-order model, a mass-damper-spring system alone can be used:

$$\ddot{\boldsymbol{\nu}}_r + 2\Delta\boldsymbol{\Omega}\dot{\boldsymbol{\nu}}_r + \boldsymbol{\Omega}^2\boldsymbol{\nu}_r = \boldsymbol{\Omega}^2 \tag{3.58}$$

.

Both models are more thoroughly discussed and elaborated in [17]. In eqs. (3.57) and (3.58), $\boldsymbol{\Delta} > 0$ and $\boldsymbol{\Omega} > 0$ are design parameters representing relative damping ratio and natural frequency, respectfully. These parameters are different for each DOF and must be tuned to achieve wanted reference trajectory. Table 3.2 display the values for $\boldsymbol{\Delta}$ and $\boldsymbol{\Omega}$ used for the different DOFs.

DOF	Δ	Ω
z_r	4	0.5
ψ_r	32	1.5
u_r	1.9	1

Table 3.2: Relative damping ratio and natural frequency for each DOF

The reference trajectories for the remaining translations (x_r, y_r), orientations (θ_r, ϕ_r), velocities (v_r, w_r), and angle rates (p_r, q_r, r_r) were calculated using the kinematic relations presented in section 3.1.1 combined with ψ_r, z_r and u_r. Some of the reference DOFs, such as the velocities v_r and w_r, are constantly zero since the wanted behavior for the REMUS 100 is to only use u together with changes in θ and ψ to change depth and heading.

3.4 Digital Twin using Core Simulation Environment

Using the CSE demo application [56], a numerical digital twin of the REMUS 100 was created. CSE is based around the functional mock-up interface (FMI). FMI defines a container and an interface to exchange dynamic models using a combination of various files, such as functional mock-up units (FMUs) [57]. Using the Simulink simulator described in section 3.3, three FMUs were exported from Simulink. For configuration of the system an SSD-file and an XML-file was written to describe which FMUs that are part of the simulation and the connections between them. A *log configurations* XML-file can also be added to specify what signals to log in each FMU.

Figure 3.6 is a screenshot of the CSE interface, while table 3.3 presents the relations between the different models.

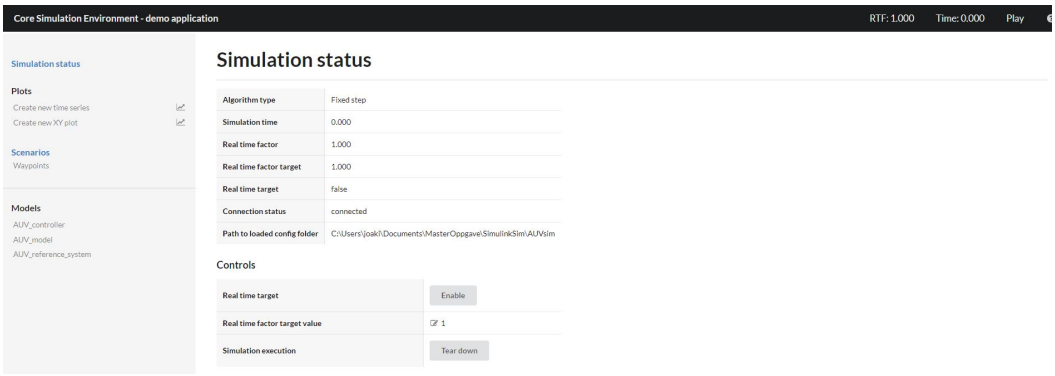

Figure 3.6: CSE interface

Models	Input	Output	Simulink block
AUV_model	tau	x	*AUV model*
AUV_controller	x_des & x	tau	*SMC*
AUV_reference_system	x	x_des	*Guidance System*

Table 3.3: CSE models with associated input/output relations

Scenarios, in the form of JSON-objects, can be added to the environment in a separate *Scenarios* folder. Each scenario event modifies a variable, making it possible to change variables at certain times. Further, the *real-time factor* value, representing the relation between simulation time and real-time, can be changed before and during the simulation.
Due to the CSE running faster than Simulink, a different sampling time had to be used when creating the FMU's. The Simulink simulator runs at 100Hz, while FMUs are generated using 1000Hz as sampling time. This may cause slight differences in the results using the DT compared to results generated by the Simulink simulator.
Further, CSE offers basic plot functionality, thus making it possible to plot the time series for model signals and local variables, as well as XY plots. This makes it easy to study input/output relations of each model, amongst other things.
The current CSE application is a demo, and the created DT is numerical. This implies that it is solely based on mathematical models of the system without using real-time data from the physical asset. In other words, the DT can't integrate sensor data from the real REMUS 100 AUV, at the current stage of the application.

Chapter 4

Experiment

In this chapter, the conducted experiment is described, and the results are presented and discussed. In 4.1, the Simulink simulation of the REMUS 100 is described, and the associated results are presented in 4.3. A discussion and comparison take place in 4.4.
Further, simulations using the DT of the REMUS 100 are presented in section 4.5, followed by a discussion regarding the benefits provided by the DT.

4.1 Simulation

Today, the control system of the physical REMUS 100 resembles a PID controller, where wanted fin angles and propeller thrust is calculated. The purpose of the simulation is to compare the designed SMC with the existing controller, as well as evaluate its robustness and ability to control 6 DOF.

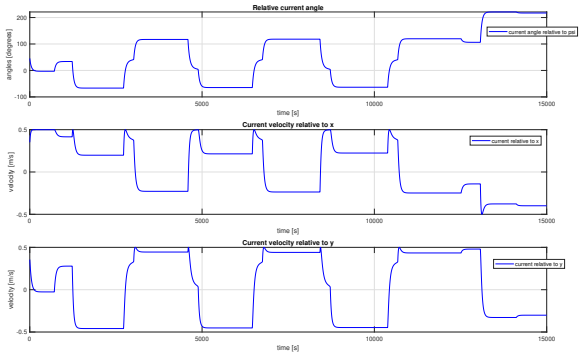

Figure 4.1: Current data relative to BODY-frame during simulation

Data gathered from a field trip involving the REMUS 100 AUV is presented in section 4.2.

For comparison reasons, the AUV in the simulation was tasked with following a trajectory similar to the one from the field trip while keeping a constant velocity. The magnitude of the current in the simulation was 0.5 m/s, and its direction was constantly 45 degrees relative to the north axis. The resulting current profile can be viewed in fig. 4.1. Table 4.1 display the waypoints given to the guidance system. Wanted velocity in surge during the simulation was set to 2 m/s.

Waypoint	**North**	**East**	**Depth**
1	0	0	2
2	1000	1000	20
3	2000	1250	20
4	1000	4000	20
5	1500	4200	25
6	2500	1250	25
7	3000	1450	25
8	2000	4400	25
9	2500	4600	12
10	3500	1450	12
11	4000	1650	20
12	3000	4800	20
13	3500	5000	20
14	4500	1500	20
15	5000	500	20
16	3000	200	2

Table 4.1: Waypoints used in simulation

4.2 Field trip results

On the 20th of November 2019, a field trip involving the REMUS 100 was organized by AUR Lab. AUR Lab develops and maintains multiple robotic platforms for marine research, including ROVs and AUVs [58]. The objective of the field trip was to map an area of the seabed nearby Munkholmen in the Trondheim fjord. Wanted velocity for the AUV, in surge, during the mission was set to 1.5 m/s.
In figs. 4.2 and 4.3, the trajectory and depth of the AUV is plotted, respectfully. Further, in figs. 4.4a and 4.4b the orientations and angle rates are given, and in fig. 4.5b the velocities are plotted, all as functions of time. fig. 4.5a displays the average current profile over the course of the mission.

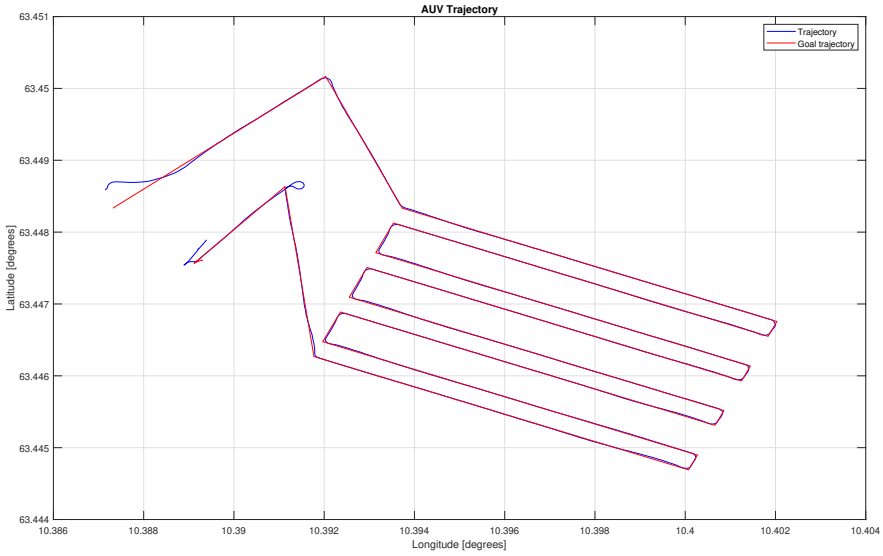

Figure 4.2: Actual longitude and latitude coordinates compared to planned mission

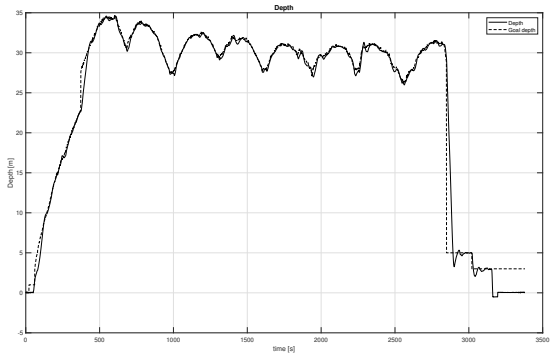

Figure 4.3: Actual depth compared to wanted depth

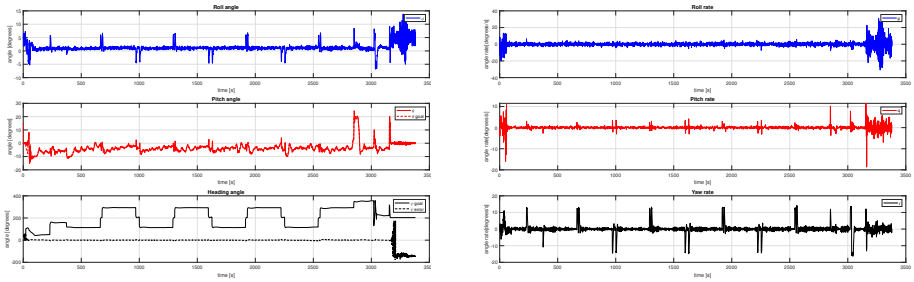

(a) Orientations as functions of time

(b) Angle rates as functions of time

Figure 4.4: Orientations and angle rates in BODY-frame

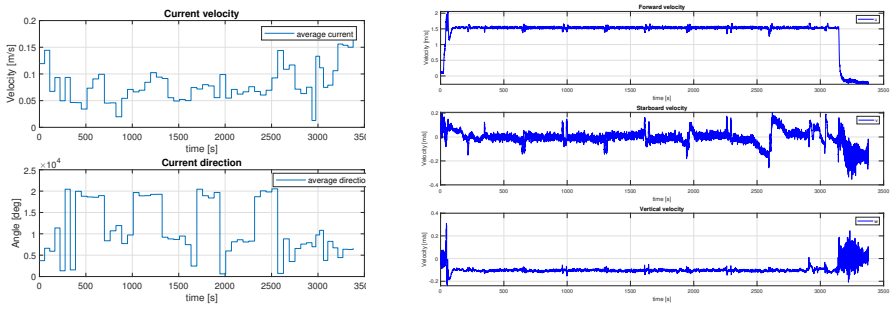

(a) Current profile

(b) Velocities in surge, sway and heave

Figure 4.5: Current profile and velocities in BODY-frame

4.3 Simulation results

The actual translations and orientations are plotted together with wanted translations and orientations in figs. 4.6 and 4.7, respectfully. Further, in fig. 4.8 the velocities and angle rates are displayed, while fig. 4.9 is a plot of wanted and actual trajectory. Lastly, in figs. 4.10 and 4.11, the translations and orientations are plotted during an interval when all DOFs are changed simultaneously.

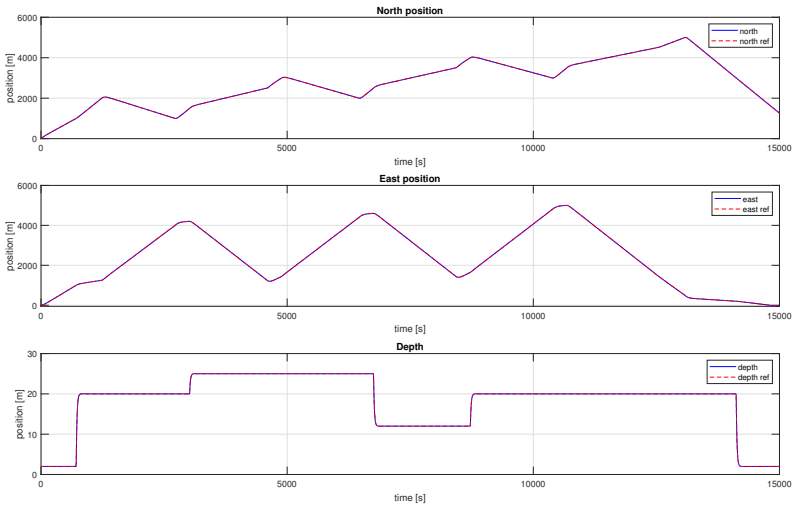

Figure 4.6: Translation of AUV relative to NED frame

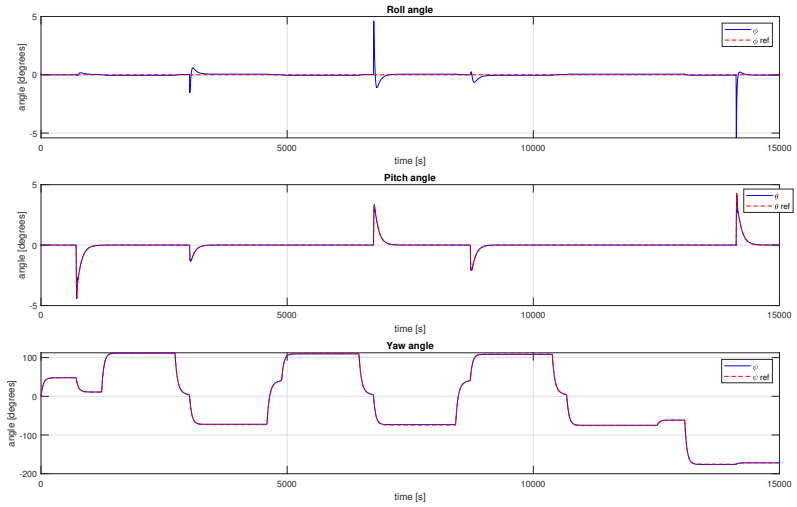

Figure 4.7: Orientation of AUV relative to NED frame

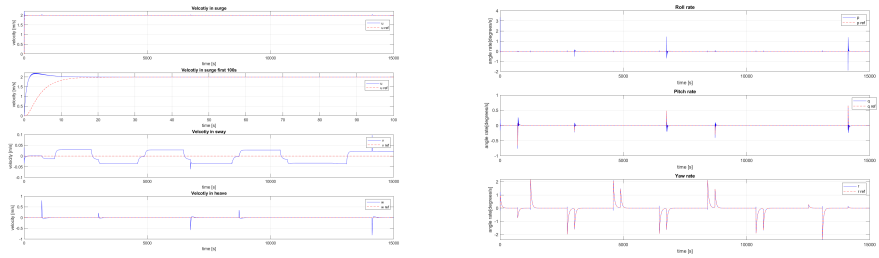

(a) Velocities

(b) Angle rates

Figure 4.8: Velocities and angle rates relative of AUV to BODY-frame

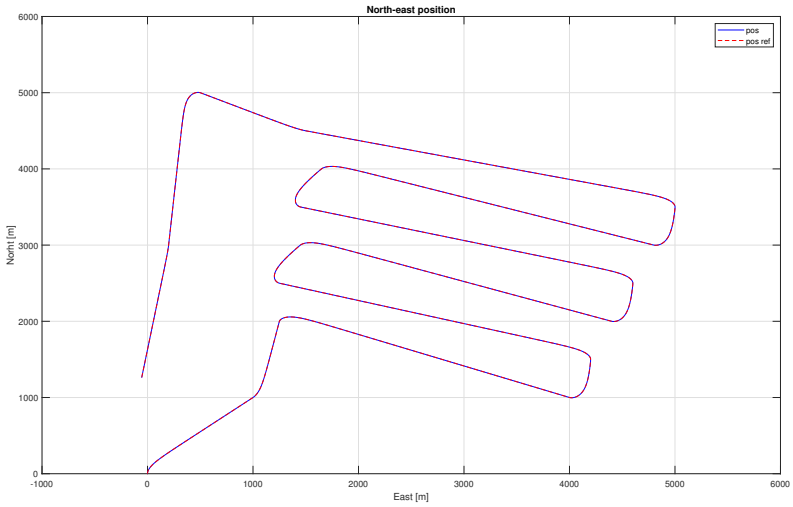

Figure 4.9: North-east position of AUV

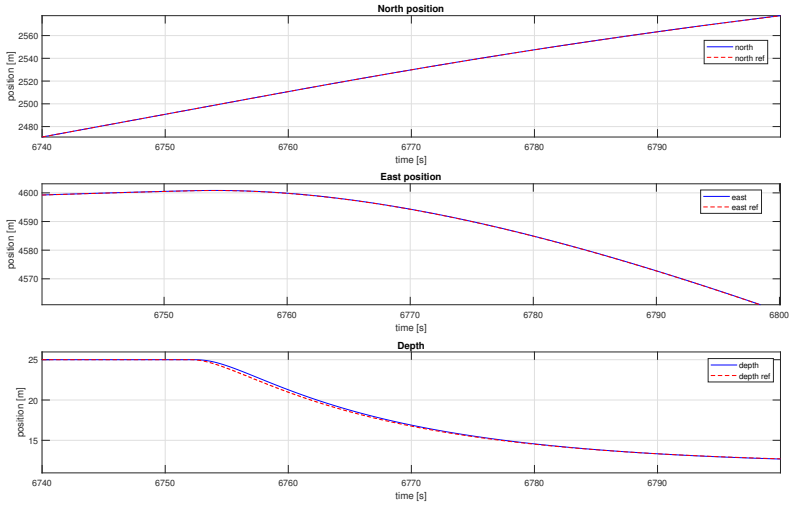

Figure 4.10: Translation of AUV relative to NED frame in interval $t \in [6740s - 6800s]$

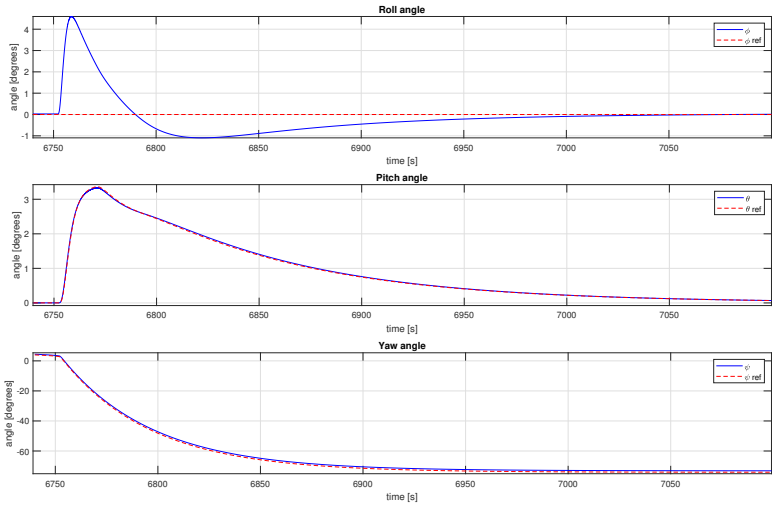

Figure 4.11: Orientation of AUV relative to NED frame in interval $t \in [6740s - 7100s]$

4.4 Discussion

Comparing fig. 4.9 to fig. 4.2, the deviance between actual and wanted trajectory is the smallest when using the SMC. The PID controller struggles in general with the corners, and during the sharp turn at a longitude degree of approximately 10.391, the AUV performs a circular motion in the opposite direction of the desired trajectory. Using the SMC a near-perfect result is achieved without any deviation from the desired trajectory. The same conclusions can be drawn when comparing the depth profiles in fig. 4.6 and fig. 4.3. Both controllers perform satisfactorily, but the SMC converges faster to the wanted depth without any overshoot. It should be noted that the depth profile in the simulation, using the SMC, is much simpler and less oscillating in the field trip. This is the result of the AUV trying to stay at 5m above seafloor during the field trip.
Studying the orientations, both controllers can generate the desired angle in pitch and yaw, but the PID encounter problems controlling the roll angle. One of the motivations behind designing a control law in 6 DOF was to deal with the unwanted roll angle and angle rate. From comparing the roll angles in fig. 4.7 and fig. 4.4a, it's evident that an improvement has been made. Due to the coupled dynamics presented in section 3.3.1, changes in pitch and yaw will lead to roll movement. The REMUS 100 only has four fins, two for steering and two for depth control, thus its not able to keep the roll at zero when turning or diving. Since the PID controller decouples the dynamics into separate systems for steering, depth, and speed, it struggles with bringing the roll angle to zero. The SMC is designed to control all DOFs and can converge the roll quickly to zero after a change in heading or depth. Same conclusions can be drawn from the angle rates in figs. 4.4b and 4.8b.
Comparing these to fig. 4.5b, where the PID controller is used, the SMC converges faster

towards wanted velocity in surge. The PID causes overshoot, then undershoot, before converging to 1.5 m/s, while the SMC quickly converges to 2 m/s within half a minute. The SMC is also less affected by the coupled motions causing deviation from wanted surge speed during changes in the AUVs orientation. Looking at the velocities in heave, we see that the PID does a better job returning the velocity to zero. This may be because the PID compensates for sideslip. The SMC controller is designed without any sideslip precautions and is therefore unable to bring the sway velocity to zero in the presence of currents, causing deviance of approximately 0,05 m/s. On the contrary, the PID experiences a similar problem in heave with a constant deviation of 0,1 m/s, while the SMC quickly converges the velocity to zero. These deviances are relatively small compared to the forward speed in surge and don't cause any major problems. They do, however, cause additional resistance for the AUV moving through the fluid and should be avoided if possible.

Since the SMC takes the highly non-linear dynamics of the AUV into consideration, it reigns superior compared to the PID-controller. As presented in section 3.3.2, the SMC without the feed-forward and robustness terms is a PD-controller. The feed-forward loop is based on knowledge about the system, thus making it capable of detecting and account for disturbances before they have time to affect the system [59]. An issue with feed-forward control is that the effects of the disturbances must be accurately predicted. The robustness term acts as a buffer for the predicted model parameters, making the SMC robust to model uncertainties. PID controllers take action only when deviance is detected, and disruption to the stable state is already in progress. In contrast, the SMC identifies the disturbance while it's still distant and computes a suitable control response.

One drawback of the SMC is that knowledge of the system dynamics is necessary to design the control law. Even though adaptive approaches exist to deal with many model uncertainties [44], some knowledge is needed to describe the dynamics. Compare that to the PID-controller, which can perform well for any process or system with proper tuning, and it's easy to understand why the PID methodology is so widely used.

Even though the SMC performs better, it is important to keep in mind that the real-life environment, in which the PID-controller operates, is more complicated and difficult to control. The Simulink simulator is a simplified model of the real world assuming perfect measurements and knowledge of the dynamics.

Another motivation behind the SMC was to control all 6 DOF simultaneously in the presence of environmental disturbances. The coupling between the DOFs makes this is challenging to achieve. Figures 4.10 and 4.11 proves that the SMC performs extremely well and is able to control each DOF. Again, the roll angle deviates from the wanted state due to coupling but quickly converges to zero. Except for the yaw angle, all other DOFs are controlled with minimal error. The yaw angle suffers small constant deviance, which again can be related to neglecting the sideslip effect when designing the control law. But since the error is less than one degree, it's of no concern and considered negligible.

The performance of the controller is not affected by the direction or magnitude of the current relative to the AUV body. This is due to the robustness term, which work as a buffer for the estimated system parameters in the feed-forward loop. Comparing the current used in the simulation to the data gathered from the field trip show that the SMC is tested using double the strength of the current in the Trondheim fjord. Additional simulations also

show that the performance of the SMC improves when lowering the strength of the current. These results reinforces the claim that the SMC is very robust against environmental disturbances and model uncertainties.

Literature often points to chattering as the main drawback of the SMC. By using the method proposed by [55] this phenomenon has been avoided completely. Instead, the low pass filter structure to the sliding surface dynamics enhance the performance of the controller. The result is minimal oscillation compared to the real-life PID application. This also reduces the wear and tear on the AUVs actuators. The low pass filter causes a phase lag of the controller, but through proper tuning, the SMC is still globally stable.

4.5 Simulations using the Digital Twin

Using the DT described in section 3.4, simulations were performed to test and explore the abilities of the DT. In figs. 4.12 and 4.13, the translations and orientations of the AUV is plotted for the first 160 seconds.

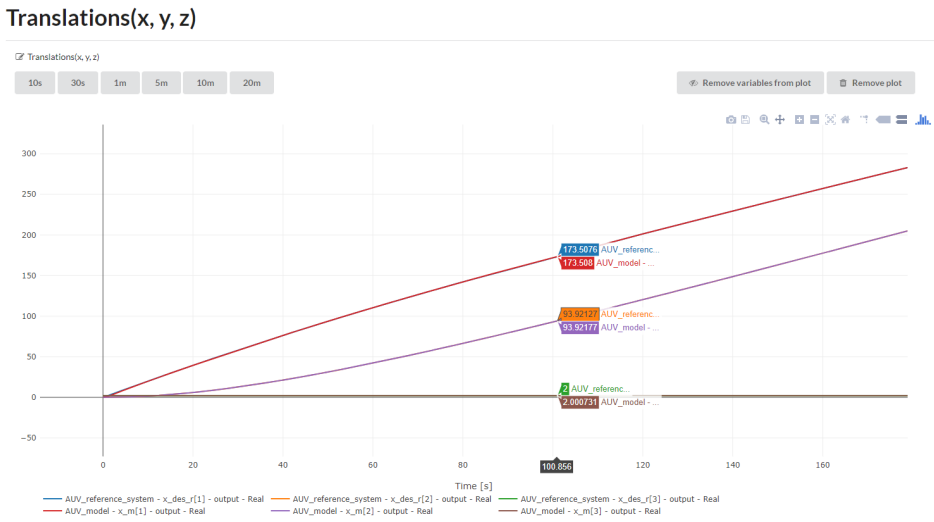

Figure 4.12: Translations during first 160 seconds of simulation

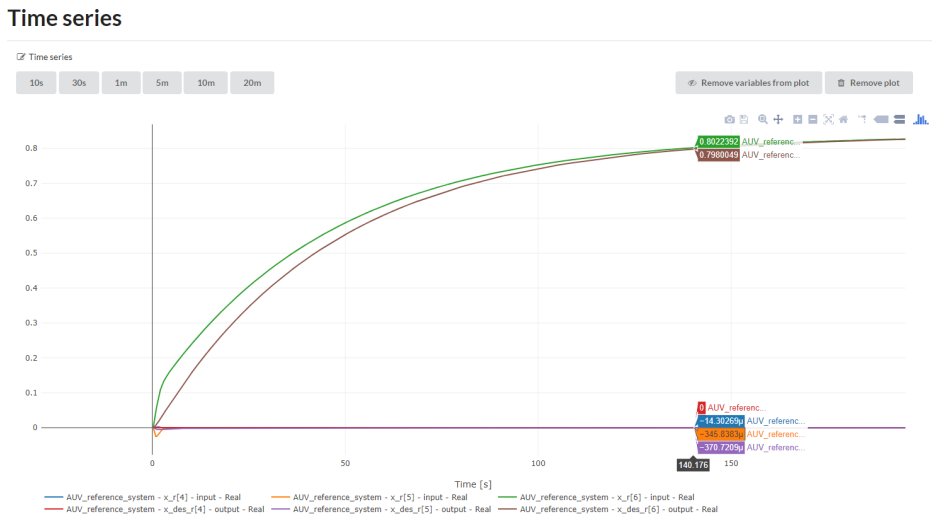

Figure 4.13: Orientations during first 160 seconds of simulation

The results obtained using the DT is more or less the same as the results presented in section 4.3. Some minimal changes occur due to the difference in sampling time, but these are negligible. Studying fig. 4.13, it can be seen that the yaw angle converges slower to the desired angle, but that the overall performance is equally good.

Further, scenarios can also be implemented. This allows the user to change different parameters or variables. For the experiment in this thesis, the most natural usage is to change the wanted trajectory. In fig. 4.14, the scenario interface, where wanted depth is changed for the second waypoint, is presented. Figure 4.15 display the resulting depth trajectory, and the results show that the AUV converges towards 30m depth instead of 20m. Each scenario can be paused or activated by clicking the button under **Actions** in the interface.

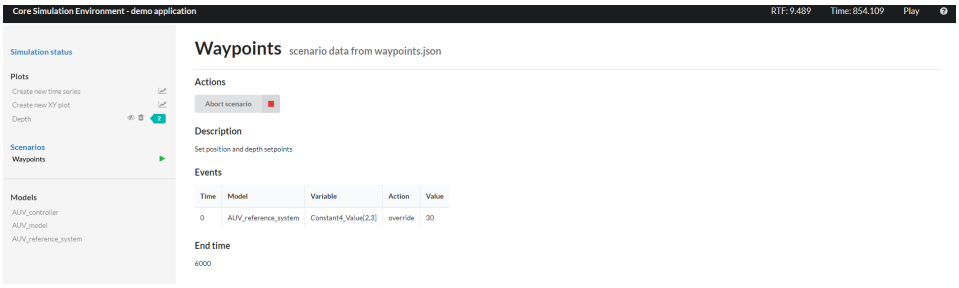

Figure 4.14: Depth scenario

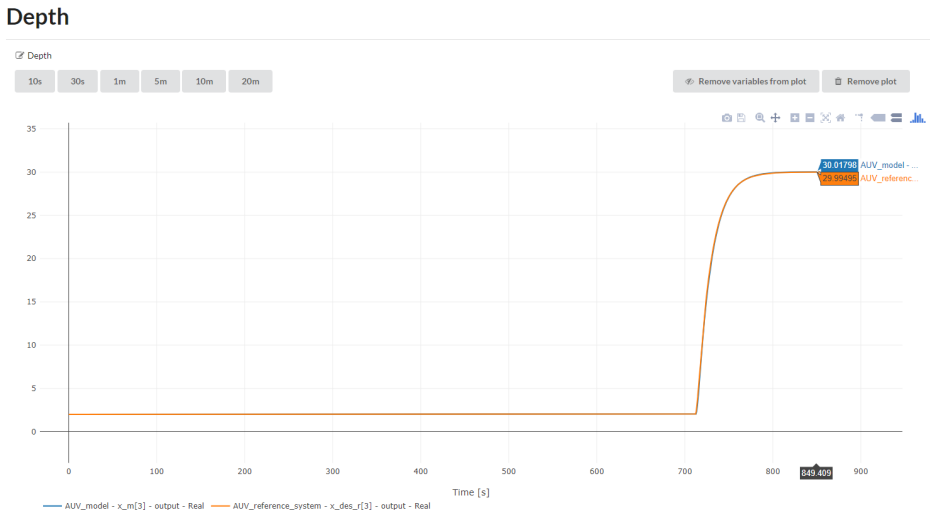

Figure 4.15: Depth when scenario is fired

The DT created using CSE is numerical and not a fully integrated real time replica of the REMUS 100. Even though many areas of usage are not applicable using this DT, it still offers many advantages. The main benefit is the environment structure using components in the form of FMUs. This makes it possible to reuse components, thus making it easier to design and build new parts of the system. Future researchers can easily test other control algorithms on the existing AUV model by importing an additional controller FMUs. In a future scenario with multiple FMUs of different controllers, guidance systems and dynamic models, the optimal solution for each system can easily be found. This will drastically increase the efficiency of the design process and reduce cost. In CSE the time series can be costumed with the desired input/output signals and model parameters, both before and during the simulation. Using hover functionality, as seen in figs. 4.12 and 4.13, the time series can easily be analysed. CSE offers a user interface more compelling to the general public and people without a technical background. Technical competence is needed to build the DT, but not to use it, which differs it from Simulink and other simulation environments. This will give a wider range of researchers the possibility to analyze and form conclusions, thus increasing the transparency of the sector.

Another advantage is the real-time factor feature of the DT. This can be useful if there are periods of peculiar behavior during a simulation that need a more precise analysis.

The major drawback of the CSE is that the FMUs are unchangeable after their creation. Depending on the structure of the FMU, some variables could be changed using scenarios. However, in the general case, it would mean that a new FMU has to be generated if an error is detected. This could slow down multiple processes if this FMU is being used in many experiments. Therefore, proper testing is important before an FMU is deployed to projects.

When finished, and CSE is an integrated part of Open Simulation Platform, it will offer the possibility to fully integrate physical assets and create high fidelity DTs. CSE will be

an open-source application which combined with the current functionality, will increase the standardization and inseparability between modeling tools and platforms. For now, however, the DT is most suitable during the design and testing phase of a systems lifecycle.

Chapter 5

Conclusions & Further Work

In this chapter conclusions are drawn and ideas for further work is presented.

5.1 Conclusion

The first objective of this thesis was to design a robust, non-linear control algorithm for the REMUS 100 capable of controlling the AUV in 6 DOF while being affected by environmental disturbances and model uncertainties. Further, this controller was to be tested using a Simulink simulator and then compared to the existing control system of the REMUS 100. The second objective was to create a DT of the REMUS 100 and explore the possible benefits a DT could provide.

Using the sliding mode methodology, a controller fulfilling the wanted criteria has been designed for the REMUS 100 and implemented in Simulink. The SMC handles the model uncertainties and environmental disturbances very well and can control all 6 DOF simultaneously. Compared to the control system on board of the REMUS 100 today, the SMC produces better results. The superior performance is a result of the predictive nature of the SMC, which is caused by the feed-forward term of the control law. This further empowers the consensus from the literature that the SMC is an excellent control method for underwater vehicles.
However, since the performed simulation study is based on mathematical models less complex than the real-life dynamics, further studies should be done before deploying the designed control law to the physical REMUS 100.

A DT has also been created using the CSE demo application, which offers a user interface that's easy to use for non-technical researchers. The interactive plot functionality, combined with scenarios and real-time factor, allow for intuitive analysis of FMU signals. The FMU structure is very useful for co-operative functionalities. It offers another dimension compared to regular Simulink simulators through the reuse of components. Systems

like CSE could increase the transparency and standardization between modeling tools and platforms in the future.

5.2 Further Work

Even though the SMC performed very well in the simulation study presented in this thesis, additional testing should be done with an emphasis on the modeling of the simulator. Imperfect measurement and state estimation are two problems associated with underwater vehicles. Therefore, to get a more realistic simulation environment, measurement noise should be implemented, as well as an observer. Since the designed controller is based on almost perfect knowledge of the REMUS 100 dynamics, it would be interesting to add more model uncertainties. Moreover, to achieve the best possible performance, sideslip should also be considered when designing the controller.

Other missions where higher precision is needed would also be interesting to perform. Since the SMC can control all 6 DOF, it has an advantage compared to linear control algorithms in scenarios like docking and collision avoidance.

Further, different approaches should be explored regarding the modeling of the DT. Instead of only using three FMUs (guidance system, model, and controller), each FMU could have been divided into smaller components. This would increase their usage in other projects and limit the potential consequences of errors. Additionally, scenarios are a feature that should be further explored during the testing and optimization of a system.
In general, since the main benefit of the system is the co-operation and reuse of components, more students and researchers should be encouraged to use the CSE demo application.

Bibliography

[1] D. Crimmins and J. Manley. (2008) What are auvs, and why do we use them? [Online]. Available: https://oceanexplorer.noaa.gov/explorations/08auvfest/background/auvs/auvs.html

[2] B. Marr. (2017, Mar.) What is digital twin technology - and why is it so important? [Online]. Available: https://www.forbes.com/sites/bernardmarr/2017/03/06/what-is-digital-twin-technology-and-why-is-it-so-important/#5d7eed432e2a

[3] K. Maritime. Autonomous underwater vehicle, remus 100. [Online]. Available: https://www.kongsberg.com/maritime/products/marine-robotics/autonomous-underwater-vehicles/AUV-remus-100/

[4] A. E. Saddik, "Digital twins: The convergence of multimedia technologies," *IEEE MultiMedia*, vol. 25, no. 2, pp. 87–92, Jun. 2018.

[5] V. Parsoya. (2019, Jul.) Why use a digital twin in the offshore world? [Online]. Available: https://www.lr.org/en-us/insights/articles/taking-advantage-of-digitalisation-why-use-a-digital-twin-in-the-offshore-world/

[6] A. Whooley. (2019, Feb.) The evolution of digital twins in subsea operations. [Online]. Available: https://www.rigzone.com/news/wire/the_evolution_of_digital_twins_in_subsea_operations-27-feb-2019-158259-article/

[7] R. Vrabic and R. Roy, "Digital twins: Understanding the added value of integrated models for through-life engineering services," *Proceedings of the 7th International Conference on Through-life Engineering Services*, vol. 16, pp. 139–146, Oct. 2018.

[8] A. Coraddu and L. Oneto, "Data-driven ship digital twin for estimating the speed loss caused by the marine fouling," *Ocean Engineering*, vol. 186, Aug. 2019.

[9] G. D. Technology. (2019) Where physical meets digital. [Online]. Available: https://defence.nridigital.com/global_defence_technology_jan19/where_physical_meets_digital_balancing_opportunity_and_risk_in_defence_in_2019

[10] S. Verma and A. Kasem. (2019) 5g a critical enabler for digitalization in oil and gas: Emerging use cases and opportunities. [Online]. Available: https://teletimesinternational.com/2019/5g-digitalization-oil-gas/

[11] DNV-GL. (2019, Jun.) Open simulation platform, taking digital twins to the next level. [Online]. Available: https://www.dnvgl.com/feature/open-simulation-platform-osp.html

[12] (2020) Open simulation platform, joint industry project for the maritime industry. [Online]. Available: https://opensimulationplatform.com/

[13] C. von Alt, "Autonomous underwater vehicles," in *Autonomous Underwater Lagrangian Platforms and Sensors Workshop*, Woods Hole Oceanographic Institution, Mar. 2003, pp. 1–5.

[14] S. Jain, "A review paper on: Autonomous underwater vehicle," *International Journal of Scientific Engineering Research*, vol. 6, no. 2, pp. 38–40, Feb. 2015.

[15] D. R. Blidberg, "The development of autonomous underwater vehicles (auv); a brief summary," Autonomous Undersea Systems Institute, Lee New Hampshire, USA, Jan. 2001.

[16] I. Tena. (2018, Apr.) The advancing technology of auvs: A view of the autonomous underwater vehicle market. [Online]. Available: https://www.hydro-international.com/content/article/the-advancing-technology-of-auvs

[17] T. I. Fossen, *Handbook of Marine Craft Hydrodynamics and Motion Control*. John Wiley Sons, Ltd, 2020.

[18] J. YUH, "Modeling and control of underwater robotic vehicles," *IEEE Transactions on Systems, Man, and Cybernetics*, vol. 20, no. 6, pp. 1475–1483, Dec. 1990.

[19] P. Egeskov and A. Bjerrum, "Design, construction and hydrodynamic testing of the auv marius," in *Proceedings of IEEE Symposium on Autonomous Underwater Vehicle Technology*, Cambridge, MA, USA, Jul. 1994, pp. 199–207.

[20] T. Prestero, "Verification of a six-degree of freedom simulation model for the remus autonomous underwater vehicle," Master's thesis, Massachusetts Institute of Technology and the Woods Hole Oceanographic Institution, Sep. 2001.

[21] Barros and Pascoal, "Auv dynamics: Modeling and paramter estimation using analytical, semi-empirical and cfd methods," *IFAC Conference on Computer Applications in Marine Systems*, vol. 37, no. 10, pp. 369–376, Jul. 2004.

[22] N. Nouri, K. Mostafapour, and S. Hassanpour, "Cfd modeling of wing and body of an auv for estimation of hydrodynamic coefficients."

[23] M. Nahon, "A simplified dynamics model for autonomous underwater vehicles," in *Proceedings of Symposium on Autonomous Underwater Vehicle Technology*.

[24] T. Prestero, “Development of a six-degree of freedom simulation model for the remus autonomous underwater vehicle,” Honolulu, HI, USA, Aug. 2001, pp. 450–455.

[25] A. Pinheiro and E. Barros, “Identification of hydrodynamic derivatives from auv "pirajuba" using extended kalman filter,” in *Symposium on Computing and Automation for Offshore Shipbuilding*, Rio Grande, Brazil, Mar. 2013, pp. 11–16.

[26] K. Kim and H. S. Choi, “Navigation and control for a test bed auv-snuuv i,” in *Proceedings of the 2004 International Symposium on Underwater Technology*, Taipei, Taiwan, Mar. 2004, pp. 89–94.

[27] E. Shahinfar and M. Bozorg, “Parameter estimation of an auv using the maximum likelihood method and a kalman filter with fading memory,” *7th IFAC Symposium on Intelligent Autonomous Vehicles*, vol. 43, no. 16, pp. 1–6, Apr. 2010.

[28] A. J. Healey and D. B. Marco, “Experimental verification of mission planning by autonomous mission execution and data visualization using the nps auv ii,” in *Proceedings of the 1992 Symposium on Autonomous Underwater Vehicle Technology*.

[29] P. Herman, “Decoupled pd set-point controller for underwater vehicles,” *Ocean Engineering*, vol. 36, no. 6-7, pp. 529–534, May 2009.

[30] M. Kokegei, F. He, and K. Sammut, “Fully coupled 6 degree-of-freedom control of an over-actuated autonomous underwater vehicle,” *Autonomous Underwater Vehicles*, pp. 147–170, Dec. 2011.

[31] K. R. G. Reshmi and P. S. Priya, “Design and control of autonomous underwater vehicle for depth control using lqr controller,” *International Journal of Science and Research (IJSR)*, pp. 1432–1436, 2013.

[32] W. Naeem, R. Sutton, and S. M. Ahmad, “Lqg/ltr control of an autonomous underwater vehicle using a hybrid guidance law,” *IFAC Workshop on Guidance and Control of Underwater Vehicles 2003*, vol. 36, no. 4, pp. 31–36, 2003.

[33] E. Y. Hong, H. G. Soon, and M. Chitre, “Depth control of an autonomous underwater vehicle, starfish,” in *OCEANS’10 IEEE SYDNEY*.

[34] R. Rout, B. Subudhi, and S. Ghosh, “Control of autonomous underwater vehicles,” Master’s thesis, Department of Electrical Engineering, National Institute of Technology, Rourkela, Odisha, India, Jan. 2013.

[35] T. I. Fossen and S. I. Sagatun, “Adaptive control of nonlinear underwater robotic system,” in *Proceedings. 1991 IEEE International Conference on Robotics and Automation*, Sacramento, CA, USA, 1991.

[36] N. Sadegh and R. Horowitz, “Stability and robustness analysis of a class of adaptive controllers for robotic manipulators,” *The International Journal of Robotics Research*.

[37] J. J. E. Slotine and M. D. D. Benedetto, “Hamiltonian adaptive control of spacecraft,” *IEEE Transactions on Automatic Control*, vol. 35, no. 7, pp. 848–852, Jul. 1990.

[38] P. Jagtap and P. Raut, "Control of autonomous underwater vehicle using reduced order model predictive control in three dimensional space," *4th IFAC Conference on Advances in Control and Optimization of Dynamical Systems ACODS 2016*, vol. 49, no. 1, p. 772–777, Feb. 2016.

[39] M. M. Hammad. (2017) Trajectory following and stabilization control of fully actuated auv using inverse kinematics and self-tuning fuzzy pid. [Online]. Available: https://doi.org/10.1371/journal.pone.0179611

[40] A. Nag, "Fuzzy logic based depth control of an autonomous underwater vehicle," in *International Mutli-Conference on Automation, Computing, Communication, Control and Compressed Sensing (iMac4s)*, Kottayam, India, 2013, pp. 117–123.

[41] B. Jalving, "The ndre-auv flight control system," *IEEE Journal of Oceanic Engineering*, vol. 19, no. 4, pp. 497–501, Oct. 1994.

[42] C. Yang, "Modular modeling and control for autonomous underwater vehicle (auv)," Master's thesis, Department of Mechanical Engineering, National University of Singapore, Apr. 2007.

[43] B. . McLain, *Small Unmanned Aircraft, Theory and Practice*. Princeton University Press, 2012.

[44] T. I. Fossen, "Nonlinear modelling and control of underwater vehicles," Master's thesis, Division of of Marine System Design, Norwegian University of Science and Technology, Trondheim, Oct. 1987.

[45] D. R. Yoerger and J.-J. Slotine, "Nonlinear control of autonomous underwater vehicles using the sliding methodology," in *OCEANS 1984*, Washington, DC, USA, Sep. 1984, pp. 588–593.

[46] K. D. Young and U. Ozguner, "Sliding mode: Control engineering in practice," San Diego, CA, USA, Aug. 1999, pp. 150–162.

[47] T. Elmokadem and M. Zribi, "Trajectory tracking sliding mode control of underactuated auvs," *Nonlinear Dynamics*, vol. 84, no. 2, pp. 1079–1091, Apr. 2016.

[48] R. Cristi, F. Papoulias, and A. Healey, "Adaptive sliding mode control of autonomous underwater vehicles in the dive plane," *IEEE JOURNAL OF OCEANIC ENGINEERING,*, vol. 15, no. 3, pp. 152–160, Jul. 1990.

[49] Y. Yang and K. Yang, "Robust trajectory control for an autonomous underwater vehicle," in *2013 MTS/IEEE OCEANS - Bergen*, Bergen, Norway, Jun. 2013.

[50] T. I. Fossen and S. I. Sagatun, "Adaptive control of nonlinear underwater robotic systems," *Modeling, Identification and Control*, vol. 12, no. 2, pp. 95–105, Apr. 1991.

[51] T. I. Fossen and O. E. Fjellstad, "Robust adaptive control of underwater vehicles: A comparative study," *3rd IFAC Workshop on Control Applications in Marine Systems*, vol. 28, no. 2, pp. 66–74, May 1996.

[52] D. R. Yoerger and J.-J. Slotine, "Adaptive sliding control of an experimental underwater vehicle," in *Proceedings. 1991 IEEE International Conference on Robotics and Automation*, vol. 3, Sacramento, CA, USA, Apr. 1991, pp. 2746–2751,.

[53] P. Norgren and R. Skjetne, "Line-of-sight iceberg edge-following using an auv equipped with multibeam sonar," *10th IFAC Conference on Manoeuvring and Control of Marine Craft MCMC 2015*, vol. 48, no. 16, pp. 81–88, Aug. 2015.

[54] V. Utkin, "Chattering problem," *IFAC Proceedings Volumes*, vol. 44, no. 1, pp. 13 374–13 379, 2011.

[55] J. J. E. Slotine and W. Li, *APPLIED NONLINEAR CONTROL*. Prentice-Hall, Inc, 1991.

[56] (May) Osp core simulation environment released for testing. [Online]. Available: https://opensimulationplatform.com/2019/05/06/osp-core-simulation-environment-released-for-testing/

[57] (2020) Fmi: Functional mock-up interface. [Online]. Available: https://fmi-standard.org/

[58] (2020) The applied underwater robotics laboratory. [Online]. Available: https://www.ntnu.edu/aur-lab

[59] D. Cooper and A. Houtz. (2015, Apr.) Feed forward with feedback trim for improved disturbance rejection. [Online]. Available: https://controlguru.com/the-feed-forward-controller/

Appendices

A Table of Coefficients

The numerical values of the coefficients presented in section 3.3.1:

Parameter	Value	Unit
$X_{\dot{x}}$	-0.93	kg
$Y_{\dot{v}}$	-35.5	kg
$Z_{\dot{w}}$	-35.5	kg
$K_{\dot{p}}$	-0.0704	kg $\cdot m^2/rad$
$M_{\dot{q}}$	-4.88	kg $\cdot m^2/rad$
$N_{\dot{r}}$	-4.88	kg $\cdot m^2/rad$
X_{uu}	-1.62	kg/m
X_{vv}	-1310	kg/m
X_{ww}	-2.86	kg/m
K_{pp}	-0.13	kg $\cdot m^2/rad^2$
M_{qq}	-188	kg $\cdot m^2/rad^2$
N_{rr}	-94	kg $\cdot m^2/rad^2$
Y_{rr}	0.632	kg $\cdot m/rad^2$
Z_{qq}	-0.632	kg $\cdot m/rad^2$
M_{ww}	3.18	kg
N_{vv}	-3.18	kg

B Barbalat's lemma

Let $\boldsymbol{s}$: $\mathbb{R}_+ \rightarrow \mathbb{R}$ be a uniformly continuous function and suppose that $lim_{t\rightarrow\infty} \int_0^t \boldsymbol{s}(\tau)ds$ exist and is finite, then

$$lim_{t\rightarrow\infty}\boldsymbol{s}(t) = 0. \tag{1}$$

C Attachments

The attached zip-file, **Attachments**, include the following two maps:

Digital Twin, which contains the files needed to configure the DT. Follow these steps to build the DT:

1. Double click on the *run-windows* command.
2. Add the location of the **Digital Twin**-map to the configuration path and press "Load simulation".
3. Read the instruction on how to use CSE by clicking the "?" in the top right corner.

Simulink Simulator, which contains the files needed to run the Simulink simulation. Follow these steps to run the simulation:

1. Open MATLAB and navigate to the **Simulink Simulator** folder.
2. Right click on the **ArcticAuvSim** folder inside SIMULINK and click "Add to path -> Selected folders and subfolders".
3. Navigate to the **AUVsim** folder.
4. Run the *run.m* script to start simulation.

NTNU

Norwegian University of
Science and Technology